Probing the Mechanism of Carbon−Hydrogen Bond Activation by Photochemically Generated Hydridotris(pyrazolyl)borato Carbonyl Rhodium Complexes: New Experimental and Theoretical Investigations

Alexander J. Blake,[†] Michael W. George,*[,†] Michael B. Hall,*[,‡] Jonathan McMaster,[†] Peter Portius,[†] Xue Z. Sun,[†] Michael Towrie,[§] Charles Edwin Webster,[⊥] Claire Wilson,[†] and Snežana D. Zarić[||]

School of Chemistry, University of Nottingham, University Park, NG7 2RD, U.K., Department of Chemistry, Texas A&M University, College Station, Texas 77843-3255, Central Laser Facility, CCLRC Rutherford Appleton Laboratory, Chilton, Didcot, Oxfordshire, OX11 0QX, U.K., Department of Chemistry, The University of Memphis, Memphis, Tennessee 38152-3550, and Department of Chemistry, University of Belgrade, Studentski trg 16, P.O. Box 158, 11001 Belgrade, Serbia

Received August 31, 2007

Fast time-resolved infrared (TRIR) experiments and density functional (DFT) calculations have been used to elucidate the complete reaction mechanism between alkanes and photolytically activated hydridotris(pyrazoly-1-yl)boratodicarbonylrhodium. TRIR spectra were obtained after photolysis of $Rh(Tp^{4\text{-}tBu\text{-}3,5\text{-}Me})(CO)_2$ in *n*-heptane, *n*-decane, and cyclohexane and of $Rh(Tp^{3,5\text{-}Me})(CO)_2$ in *n*-heptane and cyclohexane. Initial photolysis produces a coordinatively unsaturated, 16-electron monocarbonyl species that vibrationally relaxes to an intermediate with ν_{CO} of 1971 cm^{-1} in *n*-heptane solution (species **A**). DFT calculations on $Rh(Tp^{3,5\text{-}Me})(CO)-RH$ ($RH = C_2H_6$, C_6H_{12}) suggest that **A** is the triplet state of a five-coordinate, square-pyramidal $Rh(\kappa^3\text{-}Tp^{3,5\text{-}Me})(CO)-RH$, in which the alkane is weakly bound. Within the first 2 ns, a new transient grew in at 1993 cm^{-1} (species **B**). The calculations show that the observed species **B** is the singlet state of a four-coordinate $Rh(\kappa^2\text{-}Tp^{3,5\text{-}Me})(CO)(RH)$, in which the alkane is strongly bound and one pyrazolyl ring is rotated, decoordinating one N. The transient due to **B** grew at the same rate as **A** partially decayed. However, **A** did not decay completely, but persisted in equilibrium with **B** throughout the time up to 2500 ps. The ν(CO) bands due to **A** and **B** decayed at the same rate as a band at 2026 cm^{-1} grew in (τ ca. 29 ns, *n*-heptane). The latter band can be readily assigned to the final alkyl hydride products, $Rh(\kappa^3\text{-}Tp^{4\text{-}tBu\text{-}3,5\text{-}Me})(CO)R(H)$ and $Rh(\kappa^3\text{-}Tp^{3,5\text{-}Me})(CO)R(H)$ (species **D**). The experimental data do not allow the elucidation of which of the two alkane complexes, **A** or **B**, is C−H activating, or whether both of the complexes react to form the final product. The calculations suggest that a third intermediate (species **C**) is the C−H activating species, that is, the final product **D** is formed from **C** and not directly from either **A** or **B**. Species **C** is nominally a five-coordinate, square-pyramidal $Rh(\kappa^{2\,1}/_{2}\text{-}Tp^{3,5\text{-}Me})(CO)(RH)$ complex with a strongly bound alkane and one pyrazolyl partially decoordinated, but occupying the apical position of the square pyramid. Intermediate **C** is unobserved, as the calculations predict it possesses the same CO stretching frequency as the parent dicarbonyl. The unobserved species is predicted to lie on the reaction path between **A** and **B** and to be in rapid equilibrium with the four-coordinate species **B**.

Introduction

Carbon−hydrogen bond activation by transition metal complexes has been intensively studied as a means of increasing the reactivity and usefulness of simple, relatively unreactive alkanes as synthetic starting reagents.[1] One of the first successful attempts for the activation of strong alkyl C−H bonds, and for methane in particular, involved the initial photodissociation of a ligand, L′, from a cyclopentadienyl complex, MCpLL′, of a late transition metal (M = Rh or Ir), to form a coordinatively unsaturated intermediate. This reactive species subsequently attacks and oxidatively adds a C−H bond to form the alkyl hydride product, MCpL(R)H.[2] In addition to numerous studies of these Cp systems,[3] other studies have also been made on the related hydridotris(pyrazolyl)borate systems, MTpLL′.[4] The

[†] University of Nottingham.
[‡] Texas A&M University.
[§] CCLRC Rutherford Appleton Laboratory.
[⊥] The University of Memphis.
[||] University of Belgrade.

(1) (a) Labinger, J. A.; Bercaw, J. E. *Nature* **2002**, *417*, 507–514. (b) Arndtsen, B. A.; Bergman, R. G.; Mobley, T. A.; Peterson, T. H. *Acc. Chem. Res.* **1995**, *28*, 154–162. (c) Yang, H.; Kotz, K. T.; Asplund, M. C.; Wilkens, M. J.; Harris, C. B. *Acc. Chem. Res.* **1999**, *32*, 551–560. (d) Wasserman, E. P.; Moore, C. B.; Bergman, R. G. *Science* **1992**, *255*, 315–318. (e) Jones, W. D. *Acc. Chem. Res.* **2003**, *36*, 140–146. (f) Crabtree, R. H. *J. Chem. Soc., Dalton Trans.* **2001**, *2437*, 2450. (g) Jones, W. D. *Inorg. Chem.* **2005**, *44*, 4475–4484. (h) Hall, M. B.; Fan, H. J. *Adv. Inorg. Chem.* **2003**, *54*, 321–349. (i) Niu, S.; Hall, M. B. *Chem. Rev.* **2000**, *100*, 353–405. (j) Fan, Y.; Hall, M. B. *Organometallics* **2005**, *24*, 3827–3835. (k) Xavier, E. S.; De Almeida, W. B.; Da Silva, J. C. S.; Rocha, W. R. *Organometallics* **2005**, *24*, 2262–2268. (l) Bhalla, G.; Periana, R. A. *Angew. Chem., Int. Ed.* **2005**, *44*, 1540–1543. (m) Lee, K.; Legzdins, P.; Pamplin, C. B.; Patrick, B. O.; Wada, K. *Organometallics* **2005**, *24*, 638–649. (n) Bernskoetter, W. H.; Lobkovsky, E.; Chirik, P. J. *Organometallics* **2005**, *24*, 4367–4373.

10.1021/om7008217 CCC: $40.75 © 2008 American Chemical Society
Publication on Web 12/14/2007

Scheme 1. Different Coordination Modes for Tp in d^8 $TpML_2$ Systems

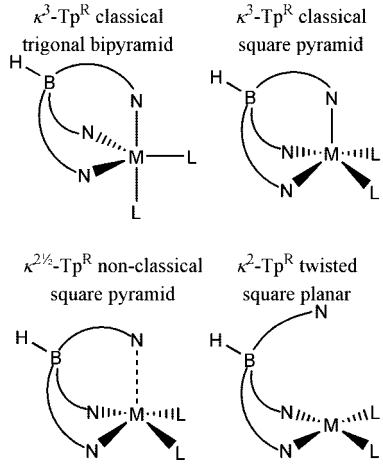

structure of these complexes depend strongly on the nature of L and L′. For example, many textbooks and papers present $Rh(Tp^{3,5\text{-}Me})(CO)_2$ as a trigonal bipyramidal structure (κ^3 structure in Scheme 1). However, a comparison of the structures and energies predicted by density functional theory (DFT) with experimental data including IR and NMR spectra show that $Rh(Tp^{3,5\text{-}Me})(CO)_2$ possesses a nonclassical square-pyramidal structure with a long Rh to N (apical ligand) bond[5] ($\kappa^{2\,1/2}$ structure in Scheme 1).

Fast time-resolved infrared (TRIR) experiments have been used to probe the initial dynamics of chemical reactions to generate a detailed picture of the mechanisms of these transformations. The first experimental observation of the reactive intermediate species that form in alkane solution with $RhTp^*(CO)_2$ ($Tp^* = Tp^{3,5\text{-}Me}$ = HB-Pz*$_3$, Pz* = 3,5-dimethylpyrazolyl) at room temperature prior to the final C−H oxidative-addition reactions was made by this technique.[6a] These and subsequent experiments[6b] resulted in TRIR spectra of the photoinitiated alkane activation reaction of $Rh(Tp^{3,5\text{-}Me})(CO)_2$ in cyclohexane solution (Scheme 2). Initial photolysis produces a coordinatively unsaturated, 16-electron monocarbonyl species that vibrationally relaxes (66 ps) to a single intermediate with ν_{CO} of 1972 cm^{-1} (species **A**). This intermediate decays with a time constant of 200 ps to a second more stable species with ν_{CO} of 1990 cm^{-1} (species **B**). The latter species in turn decays at a much slower rate to the oxidative-addition product, $Rh(\kappa^3\text{-}Tp^{3,5\text{-}Me})(CO)(R)H$ (species **D** in Scheme 2). From the experimental transient lifetimes, the effective energy barriers for the two reaction steps in the overall reaction from photochemical loss of one CO to the formation of the final alkyl hydride product, **A** → **B** and **B** → **C** → **D** (product), were estimated, where **C** denotes a postulated "activated complex", in which the C−H bond has oxidatively added to the Rh, but the third pyrazolyl ring had not yet recoordinated. Previous DFT[7] calculations predicted that the first observed intermediate (**A**) is $Rh(\kappa^3\text{-}Tp^{3,5\text{-}Me})(CO)(RH)$ with a weakly bound η^1-alkane, which subsequently rearranges to the second observed intermediate (**B**), $Rh(\kappa^2\text{-}Tp^{3,5\text{-}Me})(CO)(RH)$, a pseudosquare-planar d^8 rhodium complex with a strongly bound η^2-alkane and with one pyrazolyl ring rotated away from the metal center. The calculated ν_{CO} for the model complex for **A**, $Rh(\kappa^3\text{-}Tp)(CO)(\eta^1\text{-}CH_4)$, was 1934 cm^{-1}, while that for the model complex for **B**, $Rh(\kappa^3\text{-}Tp)(CO)(\eta^1\text{-}CH_4)$, was 1956 cm^{-1}. The predicted difference of 22 cm^{-1} is reasonably close to the observed difference of 18 cm^{-1}.

The binding of alkanes to organometallic complexes has also been probed by NMR spectroscopy. Jones and co-workers have recently performed studies to probe the selectivity of alkane activation by irradiation of $Rh(Tp^{3,5\text{-}Me})(CN\text{-neopentyl})_2$ in a mixture of two alkanes.[8] Competition studies showed the ratio of the activated complexes, which was determined by ^1H NMR spectroscopy by following the conversion of the alkyl hydrido complexes into chloro complexes. It was concluded that C−H activation of a secondary C−H bond was 10 times slower than the corresponding reaction of a primary C−H bond.[8a] Recent calculations on the related TpRh(CNR) moiety identified two alkane σ-complexes coordinated through either a methyl or methylene C−H bond, and oxidative addition was to be less favorable at the methylene C−H bond.[8b] In earlier work, Ball and co-workers were able to exploit the long lifetime of $Re(Cp)(CO)_2(alkane)$[9] to allow for a characterization of these

(2) (a) Janowicz, A. H.; Bergman, R. G. *J. Am. Chem. Soc.* **1982**, *104*, 352–354. (b) Janowicz, A. H.; Bergman, R. G. *J. Am. Chem. Soc.* **1983**, *105*, 3929–3939. (c) Hoyano, J. K. \& Graham, W. A. G. *J. Am. Chem. Soc.* **1982**, *104*, 3723–3725. (d) Hoyano, J. K.; McMaster, A. D.; Graham, W. A. G. *J. Am. Chem. Soc.* **1983**, *105*, 7190–7191. (e) Jones, W. D.; Feher, F. J. *J. Am. Chem. Soc.* **1984**, *106*, 1650. (f) Crabtree, R. H.; Mihelcic, J. M.; Quirk, J. M. *J. Am. Chem. Soc.* **1979**, *101*, 7738. (g) Crabtree, R. H.; Mellea, M. F.; Mihelcic, J. M.; Quirk, J. M. *J. Am. Chem. Soc.* **1982**, *104*, 107. (h) Watson, P. L. *J. Am. Chem. Soc.* **1983**, *106*, 6491–6493.

(3) (a) Asplund, M. C.; Snee, P. T.; Yeston, J. S.; Wilkens, M. J.; Payne, C. K.; Yang, H.; Kotz, K. T.; Frei, H.; Bergman, R. G.; Harris, C. B. *J. Am. Chem. Soc.* **2002**, *124*, 10605–10612. (b) Klei, S. R.; Golden, J. T.; Burger, P.; Bergman, R. G. *J. Mol. Catal. A: Chem.* **2002**, *189*, 79–94. (c) Golden, J. T.; Andersen, R. A.; Bergman, R. G. *J. Am. Chem. Soc.* **2001**, *123*, 5837–5838. (d) Smith, K. M.; Poli, R.; Harvey, J. N. *Chem.-Eur. J.* **2001**, *7*, 1679–1690. (e) McNamara, B. K.; Yeston, J. S.; Bergman, R. G.; Moore, C. B. *J. Am. Chem. Soc.* **1999**, *121*, 6437–6443. (f) Alaimo, P. J.; Bergman, R. G. *Organometallics* **1999**, *18*, 2707–2717. (g) Asbury, J. B.; Ghosh, H. N.; Yeston, J. S.; Bergman, R. G.; Lian, T. *Organometallics* **1998**, *17*, 3417–3419. (h) Tran, E.; Legzdins, P. *J. Am. Chem. Soc.* **1997**, *119*, 5071–5072. (i) Dunwoody, N.; Lees, A. J. *Organometallics* **1997**, *16*, 5770–5778. (j) Bromberg, S. E.; Lian, T.; Bergman, R. G.; Harris, C. B. *J. Am. Chem. Soc.* **1996**, *118*, 2069–2072. (k) Asbury, J. B.; Ghosh, H. N.; Yeston, J. S.; Bergman, R. G.; Lian, T. *Organometallics* **1998**, *17*, 3417–3419. (l) Niu, S.; Zaric, S.; Bayse, C. A.; Strout, D. L.; Hall, M. B. *Organometallics* **1998**, *17*, 5139–5147. (m) Strout, D. L.; Zarić, S.; Niu, S.; Hall, M. B. *J. Am. Chem. Soc.* **1996**, *118*, 6068–6069. (n) Bengali, A. A.; Schultz, R. H.; Moore, C. B.; Bergman, R. G. *J. Am. Chem. Soc.* **1994**, *116*, 9585–9589. (o) Rest, A. J.; Whitwell, I.; Graham, W. A. G.; Hoyano, J. K.; McMaster, A. D. *J. Chem. Soc., Dalton Trans.* **1987**, *1181*, 1190. (p) Belt, S. T.; Grevels, F. W.; Klotzbuecher, W. E.; McCamley, A.; Perutz, R. N. *J. Am. Chem. Soc.* **1989**, *111*, 8373–8382.

(4) (a) Lees, A. J.; Purwoko, A. A. *Coord. Chem. Rev.* **1994**, *132*, 155–160. (b) Purwoko, A. A.; Lees, A. J. *Inorg. Chem.* **1996**, *35*, 675–682. (c) Purwoko, A. A.; Tibensky, S. D.; Lees, A. J. *Inorg. Chem.* **1996**, *35*, 7049. (d) Pittard, K. A.; Lee, J. P.; Cundari, T. R.; Gunnoe, T. B.; Petersen, J. L. *Organometallics* **2004**, *23*, 5514–5523. (e) Bergman, R. G.; Cundari, T. R.; Gillespie, A. M.; Gunnoe, T. B.; Harman, W. D.; Klinckman, T. R.; Temple, M. D.; White, D. P. *Organometallics* **2003**, *22*, 2331–2337. (f) Ng, S. M.; Lam, W. H.; Mak, C. C.; Tsang, C. W.; Jia, G.; Lin, Z.; Lau, C. P. *Organometallics* **2003**, *22*, 641–651. (g) Tellers, D. M.; Bergman, R. G. *Organometallics* **2001**, *20*, 4819–4832. (h) Slugovc, C.; Padilla-Martinez, I.; Sirol, S.; Carmona, E. *Coord. Chem. Rev.* **2001**, *213*, 129–157.

(5) Webster, C. E.; Hall, M. B. *Inorg. Chim. Acta* **2002**, *330*, 268−282, *336*, 168.

(6) (a) Lian, T.; Bromberg, S. E.; Yang, H.; Bergman, R. G.; Harris, C. B. *J. Am. Chem. Soc.* **1996**, *118*, 3769–3770. (b) Bromberg, S. E.; Yang, H.; Asplund, M. C.; Lian, T.; McNamara, B. K.; Kotz, K. T.; Yeston, J. S.; Wilkens, M.; Frei, H.; Bergman, R. G.; Harris, C. B. *Science* **1997**, *278*, 260–263.

(7) Zarić, S.; Hall, M. B. *J. Phys. Chem. A* **1998**, *102*, 1963–1964.

(8) (a) Vetter, A. J.; Flaschenriem, C.; Jones, W. D. *J. Am. Chem. Soc.* **2005**, *127*, 12315–12322. (b) Clot, E.; Eisenstein, O.; Jones, W. D. *Proc. Nat. Acad. Sci. U.S.A.* **2007**, *104*, 6939–6944.

(9) Sun, X.-Z.; Grills, D. C.; Nikiforov, S. M.; Poliakoff, M.; George, M. W. *J. Am. Chem. Soc.* **1997**, *119*, 7521–7525.

Scheme 2. Mechanism Based on Earlier TRIR Experiments

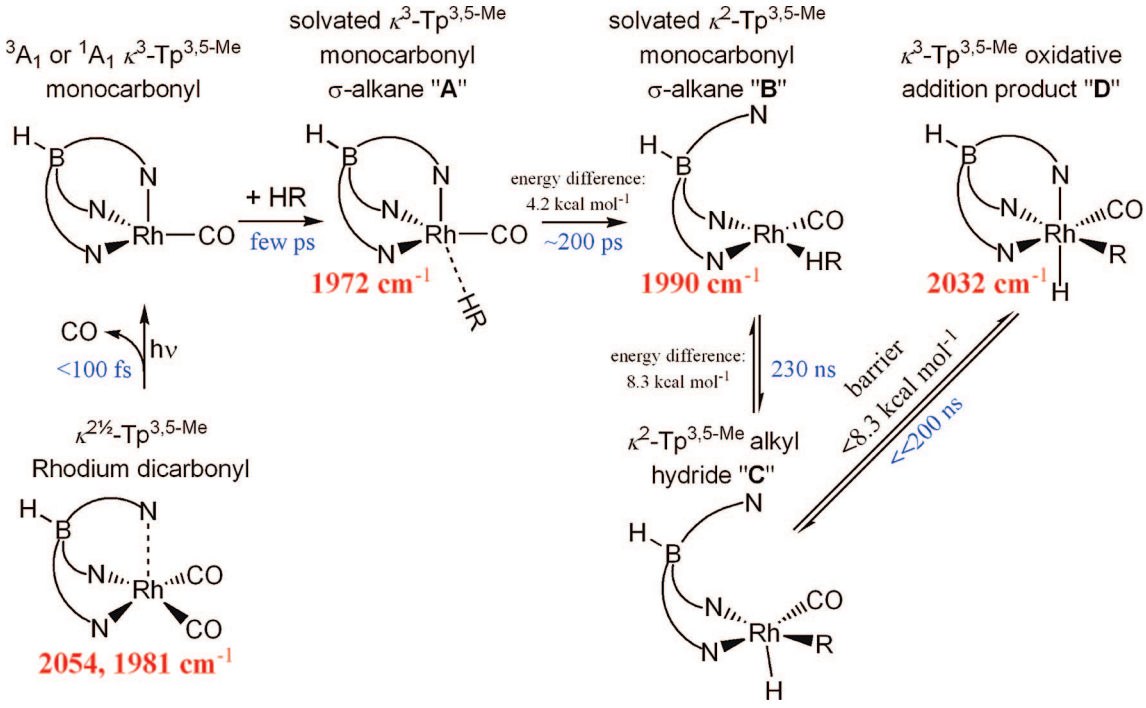

complexes by low-temperature NMR studies.[10] Although $Re(Cp)(CO)_2$(alkane) does not undergo C−H activation, studies on $Re(Cp)(CO)_2$(pentane) have provided further evidence for migration or sigmatropic rearrangements of metal−alkane bonds in organometallic alkane complexes. Three isomers, where pentane binds to the Re center via the primary $CH_3-C_4H_9$ and secondary $CH_3-CH_2-C_3H_7$ and $CH_2(C_2H_5)_2$ C−H bonds, were observed directly.[10b] For the $Re(Cp)(CO)_2$(cyclohexane) com plex a preferential binding through axial C−H bonds to the rhenium metal center was observed.[10c] A recent combined TRIR and NMR study on $Re(Cp)(CO)(PF_3)$(alkane) demonstrated that there was a rapid equilibrium between the σ-alkane complex and alkyl hydride.[11]

In this paper we build upon the initial work on Rh(Tp$^{3,5\text{-Me}}$)-$(CO)_2$ by altering the electronic and steric situation on the metal center. The photochemistry of a new ^{t}Bu-substituted complex, Rh(Tp$^{4\text{-tBu-3,5-Me}}$)$(CO)_2$, was probed using pico- and nanosecond TRIR spectroscopies. The results suggest that an alternative mechanism of C−H activation to those originally proposed[6] for Rh(Tp$^{3,5\text{-Me}}$)$(CO)_2$ may be required to explain the experimental data. We present theoretical calculations on the mechanism (structures, energies, and frequencies at critical points) of the C−H bond activation in ethane and cyclohexane by Rh-(Tp$^{3,5\text{-Me}}$)$(CO)_2$. A previous communication reported DFT results for two singlet-state intermediates only of the RhTp-$(CO)(CH_4)$ reaction.[7] Here, we address a number of unresolved issues: (1) the possibility that the ground states of the unsolvated monocarbonyl and weakly solvated monocarbonyl complexes could be triplets rather than singlets; (2) the possibility that the Tp ligands can adopt coordination modes intermediate between κ^3 and κ^2, namely $\kappa^{2½}$; (3) the nature of the final step(s) of the reaction to form the alkyl hydride product, Rh(Tp$^{3,5\text{-Me}}$)-(CO)(R)H, e.g., first oxidative addition of the C−H bond to Rh and then recoordination as originally proposed, or some other sequence of these two steps; and (4) the nature of the transition states connecting these species. This complete mapping of the critical points for the entire reaction path together with the new experimental evidence supports new conclusions about the mechanism of C−H activation.

Experimental Section

Synthesis of a New Scorpionate Ligand and the Rhodium Complex Rh(Tp$^{4\text{-tBu-3,5-Me}}$)$(CO)_2$. 3-*tert*-Butylpentane-2,4-dione[12] and 4-*tert*-butyl-3,5-dimethylpyrazol[13] were prepared according to published procedures. Synthetic work was carried out under argon using dry solvents and standard Schlenk techniques. HPLC grade alkane solvents were dried over CaH_2 and distilled prior to the experiments.

The sodium pyrazolylborate Na(Tp$^{4\text{-tBu-3,5-Me}}$) was prepared by an adaptation of the synthesis of K(Tp$^{3,5\text{-Me}}$).[14] A Schlenk tube was charged with 1.97 g (12.9 mmol) of 4-*tert*-butyl-3,5-dimethyl-pyrazole and fresh sodium borohydride (0.163 g, 4.31 mmol). This mixture was stirred and gradually heated to ca. 290 °C, while the tube was kept under a slow flow of inert gas. The hot melt produced gas, which was accompanied by gradual dissolution of the sodium borohydride. The reaction mixture was cooled, and 4-*tert*-butyl-3,5-dimethylpyrazole, which had partially condensed at the cooler parts of the apparatus, was collected at the bottom of the tube. This procedure was repeated until all solid had vanished. The product was left under high vacuum at room temperature for 3 days, resulting in a gray solid. This was dissolved in approximately 300 mL of boiling hexanes. The hot solution was filtered, and its volume was reduced by one-third, and the solution was cooled to −22 °C for 3 days. This caused precipitation of a white solid, which was collected by filtration and dried *in vacuo*, resulting in the isolation of a white powder. Yield: 552 mg, 26%. Anal. ($C_{27}H_{46}BN_6Na$,

(10) (a) Geftakis, S.; Ball, G. E. *J. Am. Chem. Soc.* **1998**, *120*, 9953–9944. (b) Lawes, D. J.; Geftakis, S.; Ball, G. E. *J. Am. Chem. Soc.* **2005**, *127*, 4134–4135. (c) Lawes, D. J.; Darwish, T. A.; Clark, T.; Harper, J. B.; Ball, G. E. *Angew. Chem.* **2006**, *45*, 4486–4490.

(11) Ball, G. E.; Brookes, C. M.; Cowan, A. J.; Darwish, T. A.; George, M. W.; Kawanami, H. K.; Portius, P.; Rourke, J. P. *Proc. Nat. Acad. Sci. U.S.A.* **2007**, *104*, 6927–6932.

(12) Lash, T. D.; Jiao, W. *J. Org. Chem.* **2003**, *68*, 3896–3901.

(13) Trofimenko, S.; Calabrese, J. C.; Thompson, J. S. *Inorg. Chem.* **1987**, *26*, 1507–1514.

(14) Trofimenko, S. *J. Am. Chem. Soc.* **1967**, *89*, 6288–6294.

Table 1. Positions of ν(CO) IR Band Maxima (cm^{-1}) of the Tris(pyrazolyl)borato Carbonyl Rhodium Species

complex	solvent	parent	κ^3-alkane complex ("**A**")	κ^2-alkane complex ("**B**")	alkyl hydride complex ("**D**")
$Rh(Tp^{4\text{-}tBu\text{-}3,5\text{-}Me})(CO)_2$	*n*-heptane	1981, 2053	1971	1993	2028.5[b]
	n-decane	1980, 2052	1970	1991	2028
	cyclohexane	1981, 2053	1971	1992	2027
$Rh(Tp^{3,5\text{-}Me})(CO)_2$	*n*-pentane	1981, 2055	1972	1992	
	n-heptane	1980, 2054			
	cyclohexane	1979, 2053			
	alkanes[a]	1981, 2054	1972	1994	2028

[a] Asplund, M. C.; Snee, P. T.; Yeston, J. S.; Wilkens, M. J.; Payne, C. K.; Yang, H.; Kotz, K. T.; Frei, H.; Bergman, R. G.; Harris, C. B., *J. Am. Chem. Soc.* **2002,** 124, 10605–12. [b] The wavenumber for the C−O stretch of $Rh(Tp^{4\text{-}tBu\text{-}3,5\text{-}Me})(CO)$(heptyl)H was determined by ns-TRIR as well as steady-state photolysis at room temperature.

488.51 g mol^{-1}) Calcd: C, 66.39; H, 9.49; N, 17.20. Found: C, 66.21; H, 9.56; N, 16.61. ^{1}H NMR (C_6D_6): δ 1.34 (27 H, s, 3 × $C(CH_3)_3$), 2.12 (9 H, s, 3 × CH_3), 2.43 (9 H, s, 3 × CH_3), 5.51 (1 H, bs, B−*H*). $^{13}C\{^1H\}$ NMR ($CDCl_3$): δ 14.3 (3 × CH_3), 16.9 (3 × CH_3), 31.4 ($C(CH_3)_3$), 32.3 ($C(CH_3)_3$), 122.1, 142.1, 145.2 (*C*-4, *C*-3 and *C*-5).

$Rh(Tp^{4\text{-}tBu\text{-}3,5\text{-}Me})(CO)_2$. A Schlenk tube was charged with 254 mg (514 μmol) of $Na(Tp^{4\text{-}tBu\text{-}3,5\text{-}Me})$ and an equimolar amount of $Rh_2Cl_2(CO)_4$ (100 mg). The mixture was suspended in dry hexanes (ca. 50 mL) at 0 °C and stirred for 15 min at ambient temperature. The volume of the reaction mixture containing a yellow suspension and a white precipitate was reduced to ca. 25 mL under reduced pressure, and the insoluble parts were filtered off. The volume of the clear yellow filtrate was reduced to ca. 5 mL, whereby precipitation of the product commenced. The solution was stored at −78 °C overnight. The canary-yellow supernatant solution was decanted off in the cold and the remainder dried *in vacuo*, which afforded ca. 0.22 g of the complex $Rh(Tp^{4\text{-}tBu\text{-}3,5\text{-}Me})(CO)_2$ as a yellow powder, yield 69%. ^{1}H NMR (C_6D_6): δ 1.10 (27 H, s, 3 × $C(CH_3)_3$), 2.49 (9 H, s, 3 × CH_3), 2.60 (9 H, s, 3 × CH_3), ca. 5.1 (1 H, bs, B−*H*). ^{1}H NMR ($CDCl_3$): δ 1.31 (27 H, s, 3 × $C(CH_3)_3$), 2.46 (9 H, s, 3 × CH_3), 2.57 (9 H, s, 3 × CH_3). For the position of the ν(CO) stretches see Table 1. UV (*n*-heptane): λ 216 nm, 265 nm, 363 nm ($\epsilon_{265} = 1.2 \times 10^3$). Anal. ($C_{29}H_{46}BN_6O_2Rh$, 624.53 g mol^{-1}) Calcd: C, 55.78; H, 7.43; N, 13.46. Found: C, 55.46; H, 7.53; N, 12.87.

Time-Resolved Infrared Spectroscopy (TRIR). Kinetic and spectroscopic studies on a time scale between 1 ps and 1 μs were performed at the PIRATE facility, situated at The Rutherford Appleton Laboratory, which has been described in detail elsewhere.[15] Picosecond-TRIR spectra were obtained using part of the output from a 1 kHz, 800 nm, 150 fs, 2 mJ Ti:Sapphire oscillator and regenerative amplifier, which was pumping a white light continuum seeded BBO OPA. The signal and idler produced by the OPA were difference frequency mixed in a type I $AgGaS_2$ crystal to generate tunable mid-infrared pulses (ca. 150 cm^{-1} fwhm, 1 μJ). Third-harmonic generation of the residual 800 nm light provided 267 nm pulses, which were used to excite the samples. Changes in the infrared absorbance were recorded by normalizing the outputs from a pair of 64-element MCT linear infrared array detectors on a shot-by-shot basis. TRIR spectra on the nanosecond time scale were obtained using a Nd:YAG laser (1 kHz) with the fs-IR laser, which operates at a 1 kHz repetition rate.[15] TRIR measurements were also performed at Nottingham using an IR diode laser TRIR spectrometer.[16] In these experiments, the change in IR transmission at one IR frequency was measured following UV excitation (266 nm), and a spectrum was built up on a point-by-point basis by repeating this measurement at different IR frequencies.

X-ray Crystallography. A suitable single crystal of $Rh(Tp^{4\text{-}tBu\text{-}3,5\text{-}Me})(CO)_2$ was obtained by the slow cooling of a concentrated solution of $Rh(Tp^{4\text{-}tBu\text{-}3,5\text{-}Me})(CO)_2$ in pentane. An orange tablet was mounted in a perfluoropolyether film atop a dual-stage glass fiber and transferred into the cold gas stream of the diffractometer. Crystal data: $C_{29}H_{46}BN_6O_2Rh$, $M = 624.44$, monoclinic, $a = 10.5252(8)$ Å, $b = 18.4639(14)$ Å, $c = 15.8470(12)$ Å, $\beta = 92.326(2)°$, $U = 3077.1(7)$ Å^3, $T = 150$ K, space group $P2_1/n$ (alt. $P2_1/c$, No. 14), $Z = 4$, μ(Mo Kα) = 0.590 mm^{-1}, 17 586 reflections measured, 7233 unique ($R_{int} = 0.031$). The final R_1 [5536 $F \geq 4\sigma(F)$] = 0.0340, wR_2 [all 7003 F^2] = 0.0776.

Computational Details. The majority of the theoretical calculations were carried out using the Gaussian98[17] and Gaussian03[18] implementations of B3LYP [the Becke three-parameter exchange functional (B3)[19] and the Lee–Yang–Parr correlation functional (LYP)[20]] and BP86 [the Becke exchange functional (B)[21] and the Perdew correlation functional (P86)[22]] density functional theory[23] with the default pruned fine grids for energies (75, 302), default pruned coarse grids for gradients and Hessians (35, 110) [neither grid is pruned for rhodium], and default SCF convergence for geometry optimizations (10^{-8}). The basis set (BS) for rhodium (341/341/31/1) in all calculations was the valence double-ζ basis set of Hay and Wadt[24] as modified by Couty and Hall (341/341/31), in which the two outermost p functions have been replaced by a (41) split of the optimized rhodium 5p function,[25] supplemented with a single set of f polarization functions;[26] this valence basis set is used in conjunction with an effective core potential. BS1 utilized the D95** basis sets of Dunning[27] for metal-ligated nitrogen, carbon, and hydrogen atoms and the D95 basis set[27] for all other atoms. BS2 replaces the polarization basis sets used for the nitrogen, carbon, and hydrogen atoms with a correlation-consistent double-ζ plus polarization basis set (cc-pVDZ)[28] and replaces all other nitrogen, carbon, boron, and hydrogen basis sets with the D95V basis sets. Each cc-pVDZ basis set has had the redundant functions removed and has been linearly transformed, as suggested by

(15) (a) Towrie, M.; Grills, D. C.; Dyer, J.; Weinstein, J. A.; Matousek, P.; Barton, R.; Bailey, P. D.; Subramaniam, N.; Kwok, W. M.; Ma, C.; Phillips, D.; Parker, A. W.; George, M. W. *Appl. Spectrosc.* **2003**, *57*, 367–380. (b) Towrie, M.; Gabrielsson, A.; Matousek, P.; Parker, A. W.; Rodriguez, A. M. B.; Vlcek, A. *Appl. Spectrosc.* **2005**, *59*, 467–473.

(16) George, M. W.; Poliakoff, M.; Turner, J. J. *Analyst* **1994**, *119*, 551–560.

(17) Frisch, M. J.; et al. *Gaussian 98, Revisions A.6, A.7, A.9, and A11.3*; Gaussian, Inc.: Pittsburgh, PA, 1998.

(18) Frisch, M. J.; et al. *Gaussian 03, Revisions B. and B.05*; Gaussian, Inc.: Wallingford, CT, 2004.

(19) Becke, A. D. *J. Chem. Phys.* **1993**, *98*, 5648–5652.

(20) Lee, C.; Yang, W.; Parr, R. G. *Phys. Rev. B* **1988**, *37*, 785–789.

(21) Becke, A. D. *Phys. Rev. A* **1988**, *38*, 3098–3100.

(22) Perdew, J. P. *Phys. Rev. B* **1986**, *33*, 8822−8824; *Phys. Rev. B* **1986**, *33*, 7406−7406.

(23) Parr, R. G.; Yang, W. *Density Functional Theory of Atoms and Molecules*; Oxford University Press: New York, 1989.

(24) (a) Hay, P. J.; Wadt, W. R. *J. Chem. Phys.* **1985**, *82*, 270–283. (b) Wadt, W. R.; Hay, P. J. J. *Chem. Phys.* **1985**, *82*, 284–298.

(25) Couty, M.; Hall, M. B. *J. Comput. Chem.* **1996**, *17*, 1359–1370.

(26) Ehlers, M.; Böhme, A. W.; Dapprich, S.; Gobbi, A.; Höllwarth, A.; Jonas, V.; Köhler, K. F.; Stegmann, R.; Veldkamp, A.; Frenking, G. *Chem. Phys. Lett.* **1993**, *208*, 111–114.

(27) Dunning, T. H.; Hay, P. J. In *Modern Theoretical Chemistry*; Schaefer, H. F., III, Ed.; Plenum: New York, 1976; pp 1–28.

(28) (a) Dunning, T. H. *J. Chem. Phys.* **1989**, *90*, 1007–1023. (b) Woon, D. E.; Dunning, T. H., Jr. *J. Chem. Phys.* **1994**, *100*, 2975–2988.

Davidson.[29] BS1 was used for the B3LYP and BP86 calculations of the $Tp^{3,5\text{-}Me}$/ethane system, while BS2 was used for the B3LYP calculations for the $Tp^{3,5\text{-}Me}$/cyclohexane system. Spherical harmonic d and f functions were used throughout; that is, there are five angular basis functions per d function and seven angular basis functions per f function.

A c-shell script combined with a Fortran-77 program[30] was used to optimize the geometry of the minimum energy crossing point (MECP) between potential energy surfaces of the singlet and triplet $Rh(Tp^{3,5\text{-}Me})(CO)(C_2H_6)$ complexes, ^{1}**3** and ^{3}**3**, respectively. This program is designed to interact directly with Gaussian.

All structures were fully optimized, and analytical frequency calculations were performed on all structures (except the MECP) to ensure that either a minimum or first-order saddle point was achieved. The calculations of the structure of $Rh(Tp^{4\text{-}tBu\text{-}3,5\text{-}Me})(CO)_2$ and, for comparison, of $Rh(Tp^{3,5\text{-}Me})(CO)_2$ were carried out at Nottingham using the Amsterdam Density Functional (ADF) suite version 2004.01.[31] The restricted relativistic DFT calculations employed a Slater-type orbital (STO) triple-ζ-plus one polarization function basis set from the ZORA/TZP database of the ADF suite for all atoms. Scalar relativistic (SR) approaches were used within the ZORA Hamiltonian for the inclusion of relativistic effects. The local density approximation (LDA) with the correlation potential due to Vosko et al. together with gradient corrections using the functionals of Becke and Perdew (BP) were used in all of the ADF DFT calculations.[32]

Results

Molecular Structure of $Rh(Tp^{4\text{-}tBu\text{-}3,5\text{-}Me})(CO)_2$. The molecular structure of $Rh(Tp^{4\text{-}tBu\text{-}3,5\text{-}Me})(CO)_2$ is shown in Figure 1. $Rh(Tp^{4\text{-}tBu\text{-}3,5\text{-}Me})(CO)_2$ possesses a distorted square-pyramidal coordination sphere about the Rh center, where the tridentate $HB(4\text{-}^tBu\text{-}3,5\text{-}Me_2Pz)_3$ ($Tp^{4\text{-}tBu\text{-}3,5\text{-}Me}$) coordinates in an asymmetric ($\kappa^{2^1/_2}$) fashion with two short Rh−N bonds (*ca*. 2.13 and 2.11 Å) and a long bond (*ca*. 2.43 Å). The structure is consistent with analogous dicarbonyl rhodium complexes.[5,33] We have used DFT calculations on $Rh(Tp^{3,5\text{-}Me})(CO)_2$ and $Rh(Tp^{4\text{-}tBu\text{-}3,5\text{-}Me})(CO)_2$ in an attempt to probe any differences in the geometric and electronic structures of these compounds. Geometry optimizations of $Rh(Tp^{3,5\text{-}Me})(CO)_2$ and $Rh(Tp^{4\text{-}tBu\text{-}3,5\text{-}Me})(CO)_2$ converge to yield coordination spheres about the Rh atoms that are almost identical. Thus, it appears that in the ground state the inclusion of electron-donating 4-tBu substituents within the $Tp^{3,5\text{-}Me}$ framework does not substantially modify the ligand–metal bonding.

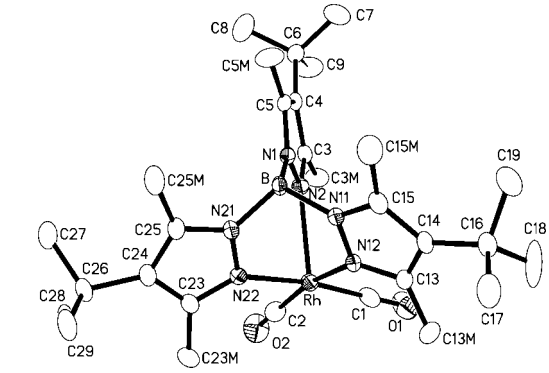

Figure 1. Representation of the molecular structure of $Rh(Tp^{4\text{-}tBu\text{-}3,5\text{-}Me})(CO)_2$, obtained by single-crystal X-ray diffraction. Displacement ellipsoids are drawn at the 50% probability level. Hydrogen atoms are omitted. Important *interatomic distances* (Å): Rh−C1 = 1.838(3), Rh−C2 = 1.842(3), Rh−N2 = 2.4317(18), Rh−N12 = 2.1261(18), Rh−N22 = 2.1111(18), C1−O1 = 1.141(3), C2−O2 = 1.138(3), B−N1 = 1.532(3), B−N11 = 1.550(3), B−N21 = 1.560(3), and *valence angles* (deg): C1−Rh−C2 = 86.04(11), C1−Rh−N2 = 104.17(9), C1−Rh−N12 = 93.59(10), C1−Rh−N22 = 171.18(10), C2−Rh−N2 = 107.32(9), C2−Rh−N12 = 168.17(9), C2−Rh−N22 = 94.33(9), N12−Rh−N2 = 84.25(6), N22−Rh−N2 = 84.16(6), N22−Rh−N12 = 84.24(7), O1−C1−Rh = 178.5(3), O2−C2−Rh = 178.3(2).

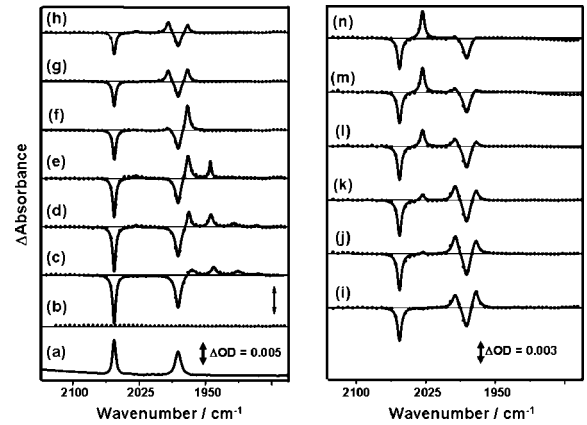

Figure 2. (a) FTIR and time-resolved spectra on the picosecond (left) and nanosecond time scale (right) of a carbon monoxide saturated solution of $Rh(Tp^{4\text{-}tBu\text{-}3,5\text{-}Me})(CO)_2$ in *n*-heptane obtained (b) –20 ps, (c) 2 ps, (d) 10 ps, (e) 30 ps, (f) 100 ps, (g) 500 ps, (h) 2 ns, (i) 1 ns, (j) 4 ns, (k) 10 ns, (l) 30 ns (m) 70 ns, and (n) 600 ns after 267 nm excitation.

TRIR Spectra. The TRIR spectra were obtained after photolysis of $Rh(Tp^{4\text{-}tBu\text{-}3,5\text{-}Me})(CO)_2$ in *n*-heptane, *n*-decane, and cyclohexane and of $Rh(Tp^{3,5\text{-}Me})(CO)_2$ in *n*-heptane and cyclohexane. Figure 2 shows the TRIR spectra obtained after photolysis (266 nm) of $Rh(Tp^{4\text{-}tBu\text{-}3,5\text{-}Me})(CO)_2$ in *n*-heptane saturated under 1 atm of CO. It is clear that the laser flash causes the instantaneous bleach of the ν(CO) bands of $Rh(Tp^{4\text{-}tBu3,5\text{-}Me})(CO)_2$ at 1981 and 2053 cm^{-1}. From the IR spectrum obtained 2 ps after photolysis several transient bands appear, which show similarity to those obtained previously by Bergman and co-workers,[6] with the related complex $Rh(Tp^{3,5\text{-}Me})(CO)_2$, Table 1. We adopted their nomenclature (Scheme 2) for the intermediates formed during the reaction. The band observed at 1971 cm^{-1} can be assigned to the alkane complex $Rh(\kappa^3\text{-}Tp^{4\text{-}tBu\text{-}3,5\text{-}Me})(CO)$(heptane) (**A**), whereas the three bands at lower energy are believed to arise from vibrationally and/or electronically excited states of

(29) Davidson, E. R. *Chem. Phys. Lett.* **1996**, *260*, 514–518.

(30) (a) Harvey, J. N.; Aschi, M.; Schwarz, H.; Koch, W. *Theor. Chem. Acc.* **1998**, *99*, 95. (b) Harvey, J. N.; Aschi, M. *Phys. Chem. Chem. Phys.* **1999**, *1*, 5555–5563. (c) Harvey, J. N. *J. Am. Chem. Soc.* **2000**, *122*, 12401–12402. (d) Harvey, J. N. In *Spin-Forbidden Reactions in Transition-Metal Chemistry*; Cundari, T. R., Ed.; Marcel Dekker, Inc.: New York, 2001. (e) Smith, K. M.; Poli, R.; Harvey, J. N. *Chem.-Eur. J.* **2001**, *7*, 1679–1690. (f) Smith, K. M.; Poli, R.; Harvey, J. N. *New J. Chem.* **2000**, *24*, 77–80. (g) Carreon-Macedo, J. L.; Harvey, J. N. *J. Am. Chem. Soc.* **2004**, *126*, 5789–5797.

(31) (a) Fonseca Guerra, C.; Snijders, J. G.; Velde, G. T.; Baerends, E. J. *Theor. Chem. Acc.* **1998**, *99*, 391–403. (b) Velde, G. T.; Bickelhaupt, F. M.; van Gisbergen, S. J. A.; Fonseca Guerra, C.; Baerends, E. J.; Snijders, J. G.; Ziegler, T. *J. Comput. Chem.* **2001**, *22*, 931–967.

(32) Vosko, S. H.; Wilk, L.; Nusair, M. *Can. J. Phys.* **1980**, *58*, 1200–1211.

(33) (a) Ohta, K.; Hashimoto, M.; Takahashi, Y.; Hikichi, S.; Akita, M.; Moro-oka, Y. *Organometallics* **1999**, *18*, 3234–3240. (b) Del Ministro, E.; Renn, O.; Rueegger, H.; Venanzi, L. M.; Burckhardt, U.; Gramlich, V. *Inorg. Chim. Acta* **1995**, *240*, 631–639. (c) Rheingold, A. L.; Ostrander, R. L.; Haggerty, B. S.; Trofimenko, S. *Inorg. Chem.* **1994**, *33*, 3666–3676. (d) Moszner, M.; Wolowiec, S.; Trosch, A.; Vahrenkamp, H. *J. Organomet. Chem.* **2000**, *595*, 178–185.

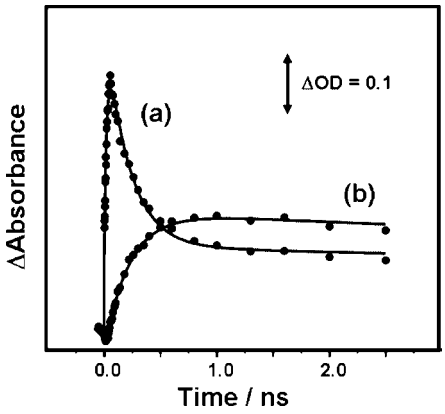

Figure 3. TRIR traces of the (a) decay of Rh(κ^3-Tp$^{4\text{-tBu-3,5-Me}}$)(CO)(heptane) and (b) rise and partial decay of Rh(κ^2-Tp$^{4\text{-tBu-3,5-Me}}$)(CO)(heptyl)H (1971 cm^{-1}) obtained following photolysis of Rh(κ^3-Tp$^{4\text{-tBu-3,5-Me}}$)(CO)$_2$ in the carbon monoxide saturated solution.

Rh(κ^3-Tp$^{4\text{-tBu-3,5-Me}}$)(CO)$_2$ and Rh(κ^3-Tp$^{4\text{-tBu-3,5-Me}}$)(CO)(heptane). Within the first 100 ps these bands have completely decayed, the ν(CO) band due to **A** has increased in intensity and the parent ν(CO) bands have partially recovered.[34] The yield for the CO loss channel (calculated using the extent of Rh(κ^3-Tp$^{4\text{-tBu-3,5-Me}}$)(CO)$_2$ reformation) amounts to 52%. A significant amount of the parent bleach (48%) has recovered within the first 200 ps. Within the first 2 ns of our experiment a new transient grew in at 1993 cm^{-1}. This transient grew at the same rate as **A** partially decayed (τ = 236 ($\pm$12) ps); see Figure 3. It is important to note that **A** did not decay completely, but persisted throughout the time up to 2500 ps. By comparison with the previous TRIR results,[6] the second intermediate, at 1993 cm^{-1}, can be assigned to Rh(κ^2-Tp$^{4\text{-tBu-3,5-Me}}$)(CO)(heptane) (**B**), where one arm of the polydentate ligand has completely dechelated.

The ν(CO) bands due to **A** and **B** decayed at the same rate as a band at 2028.5 cm^{-1} grew in (τ = 28.8 ($\pm$0.5) ns). The latter band can be readily assigned to the final product Rh(κ^3-Tp$^{4\text{-tBu-3,5-Me}}$)(CO)H(heptyl) (**D**) by analogy with previous TRIR experiments, Figure 2. These observations are in marked contrast to results obtained with Rh(Tp$^{3,5\text{-Me}}$)(CO)$_2$ in pure alkane solution, where a complete conversion of Rh(κ^3-Tp$^{3,5\text{-Me}}$)(CO)(alkane) (**A**) into Rh(κ^2-Tp$^{3,5\text{-Me}}$)(CO)(alkane) (**B**) was observed,[6] the latter complex decaying to form Rh(κ^3-Tp$^{3,5\text{-Me}}$)(CO)(alkyl)H (**D**). Furthermore, in our experiments, a partial recovery (ca. 15%) of the parent bleaches was observed on the same time scale as that for the C$-$H activation. Although there are significant differences from the photochemistry of Rh(Tp$^{3,5\text{-Me}}$)(CO)$_2$ in alkane solvents, there are some similarities to the results reported for liquefied xenon at cryogenic temperatures, where photolysis of Rh(Tp$^{3,5\text{-Me}}$)(CO)$_2$ generated Rh(κ^3-Tp$^{3,5\text{-Me}}$)(CO)Xe and Rh(κ^2-Tp$^{3,5\text{-Me}}$)(CO)Xe in approximately equal concentration.[35] Our results suggest that Rh(κ^3-Tp$^{4\text{-tBu-3,5-Me}}$)(CO)(heptane) (**A**) is formed initially and decays to produce an equilibrium mixture involving Rh(κ^3-Tp$^{4\text{-tBu-3,5-Me}}$)(CO)(heptane) (**A**) $\leftrightarrow$ Rh(κ^2-Tp$^{4\text{-tBu-3,5-Me}}$)(CO)(heptane) (**B**). In the presence of CO the constituents of this equilibrium undergo parallel reactions recombining with free CO to reform Rh(Tp$^{4\text{-tBu-3,5-Me}}$)(CO)$_2$ and activating C$-$H bonds to form Rh(κ^3-Tp$^{4\text{-tBu-3,5-Me}}$)(CO)H(heptyl) (**D**).

The irradiation of Rh(Tp$^{4\text{-tBu-3,5-Me}}$)(CO)$_2$ in either *n*-decane or cyclohexane gave picosecond TRIR spectra similar to those described above for *n*-heptane, Figure 4. However, there are several significant differences in the photochemical behavior of Rh(Tp$^{4\text{-tBu-3,5-Me}}$)(CO)$_2$ in the latter solvents. The reactions in *n*-decane are very similar to those in *n*-heptane except that the time taken to establish the equilibrium between **A** and **B** was slightly longer (*ca.* 2000 ps vs 500 ps). The formation of **D** occurs at a similar rate (34.3 $\pm$ 0.3 ns) as the formation of **D** with *n*-heptane (28.8 $\pm$ 0.5 ns). In cyclohexane, however, the formation of **D** was almost 6 times slower (199 $\pm$ 12 ns) compared to the other alkanes in the presence of CO. Although the equilibrium between **A** and **B** was established on a similar time scale for all three alkane complexes (1–2 ns), the equilibrium ratios of **A** vs **B** were slightly different (*n*-heptane, 5:7; *n*-decane, 11:12; and cyclohexane, 1:2).

Another key difference observed in cyclohexane is that, in the presence of CO, the decay of **A** to form **D** is a minor pathway and reformation of Rh(Tp$^{4\text{-tBu-3,5-Me}}$)(CO)$_2$ dominates; that is, the reaction of the cyclohexane complex with CO is favored. The rate of formation and the yield of **D** were found to be very sensitive to the CO concentration. The rate of **D** formation was measured (k_{obs} = 9.5 $\times$ 10^5 s^{-1}) without added CO. During the course of C$-$H activation the extent of parent recovery was minor (<10%), and therefore k_{obs} is a good estimate for the rate of C$-$H activation. Thus, the cyclohexyl hydride complex is formed on a much slower time scale (τ ca. 1 μs) compared to alkane complexes in solution with linear alkanes, Figure 5. At higher CO concentrations (e.g., 2.3 $\times$ 10^{-3} mol dm^{-3}) the observed rate increased by more than 1 order of magnitude (k_{obs} = 1.1 $\times$ 10^7 s^{-1}), whereas the yield of the C$-$H activated product **D** decreased significantly. A higher CO concentration increases the extent of parent reformation. We have used the latter dependence to approximate the bimolecular rate constant for the reaction of the equilibrium mixture with CO, (5.9 $\pm$ 0.4) $\times$ 10^8 dm^3 mol^{-1} s^{-1}. We have also performed a similar experiment for Rh(Tp$^{3,5\text{-Me}}$)(CO)$_2$, and a smaller rate constant was found, (2.6 $\pm$ 0.1) $\times$ 10^8 dm^3 mol^{-1} s^{-1}, which indicates that the presence of the ^{t}Bu groups increases the reactivity of the alkane complex slightly in the reaction with CO.

The rate of C$-$H activation in cyclohexane is much slower than in those *n*-alkanes described above (see Figure 4) and appears also to be slower than the rate reported for the rearrangement of Rh(κ^2-Tp$^{3,5\text{-Me}}$)(CO)(cyclohexane) (**B**) to Rh(κ^3-Tp$^{3,5\text{-Me}}$)(CO)(cyclohexyl)H (**D**).[6] However, a good estimate of the lifetime for Rh(κ^2-Tp$^{3,5\text{-Me}}$)(CO)(alkane) (**B**) was not reported, preventing a direct comparison of the reactivity of Rh(κ^2-Tp$^{3,5\text{-Me}}$)(CO)(*n*-alkane) in a *n*-alkane solvent[6] with the results described above. We therefore repeated the TRIR measurement for intermediates **B** with Tp$^{3,5\text{-Me}}$ ligand for both *n*-heptane and cyclohexane and determined that the rate of C$-$H activation is much faster for *n*-heptane (τ = 6 ns) compared to cyclohexane (τ = 240 ns). Thus, for both starting complexes, Rh(κ^3-Tp$^{4\text{-tBu-3,5-Me}}$)(CO)$_2$ and Rh(κ^3-Tp$^{3,5\text{-Me}}$)(CO)$_2$, the rate of C$-$H activation is significantly slower (ca. 30 to 40 times) for the cyclic alkanes.

Activation Parameters. Experimentally determined activation parameters are given in Table 2. The enthalpies of C$-$H activation for the formation of **D** for Rh(κ^3-Tp$^{4\text{-tBu-3,5-Me}}$)(CO)(alkyl)H are alkyl = heptyl (2.9 kcal mol^{-1}) and cyclohexyl (4.9 kcal mol^{-1}), and those for Rh(κ^3-Tp$^{3,5\text{-Me}}$)(CO)(alkyl)H

(34) There is also a broad and overlapped band at 2040 cm^{-1}, which decayed on a similar time scale. The origin of this band is still unclear.

(35) Yeston, J. S.; McNamara, B. K.; Bergman, R. G.; Moore, C. B. *Organometallics* **2000**, *19*, 3442–3446.

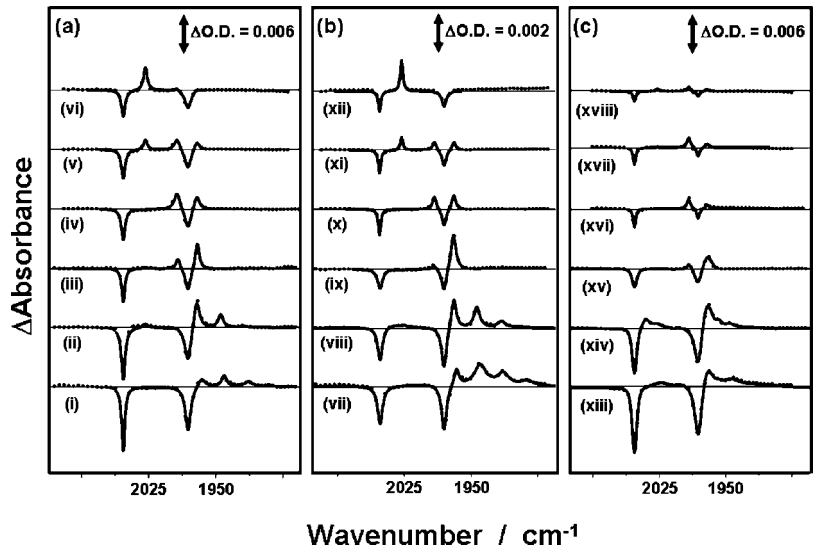

Figure 4. Selected nanosecond- and picosecond-TRIR spectra in carbon monoxide saturated solutions of $Rh(Tp^{4\text{-tBu-3,5-Me}})(CO)_2$ in (a) *n*-heptane ((i) 2 ps, (ii) 20 ps, (iii) 200 ps, (iv) 2 ns, (v) 20 ns, and (vi) 200 ns); (b) *n*-decane ((vii) 2 ps, (viii) 20 ps, (ix) 200 ps, (x) 2 ns, (xi) 20 ns, and (xii) 220 ns); and (c) cyclohexane ((xiii) 2 ps, (xiv) 22 ps, (xv) 200 ps, (xvi) 2 ns, (xvii) 20 ns, and (xviii) 200 ns) after 267 nm excitation.

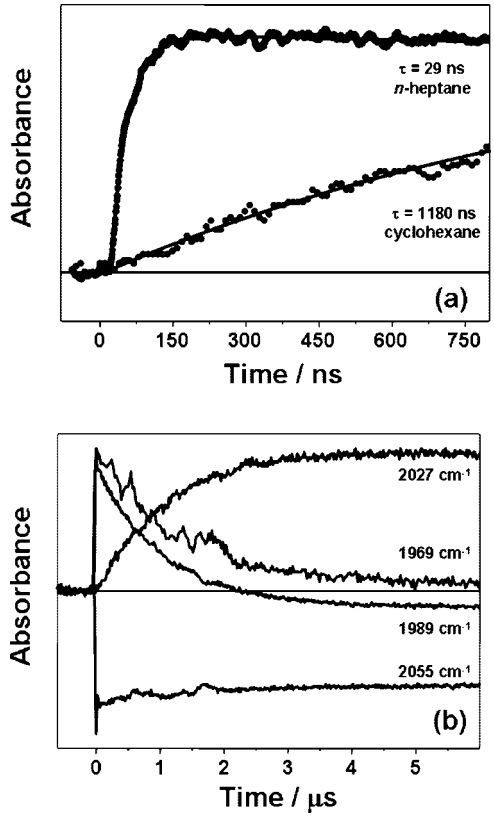

Figure 5. (a) Diode laser TRIR traces of the C−H activated products $Rh(Tp^{4\text{-tBu-3,5-Me}})(CO)$(heptyl)H and $Rh(Tp^{4\text{-tBu-3,5-Me}})$-(CO)(cyclohexyl)H in the absence of added carbon monoxide showing the marked difference in rate constants of C−H activation in *n*-heptane or cyclohexane. The two traces have been normalized to rise to $\Delta A = 1$ at infinite time. (b) Superposition of the transients and the parent bleach in cyclohexane, showing the concomitant rise of the C−H activated complex and decay of both complexes in the same solvent.

are alkyl = pentyl (4.0 kcal mol^{-1}), decyl (3.2 kcal mol^{-1}), and cyclohexyl (5.1 kcal mol^{-1}). As expected from the rates, the C−H activation enthalpies for the formation of Rh(Tp′)-(CO)(cyclohexyl)H was significantly higher than those for Rh(Tp′)(CO)(heptyl)H (Tp′ = κ^3-$Tp^{4\text{-tBu-3,5-Me}}$ or κ^3-$Tp^{3,5\text{-Me}}$), Table 2. The larger C−H activation enthalpies for cyclohexane than for linear alkanes for both complexes indicate that both ($Rh(\kappa^3\text{-}Tp^{4\text{-tBu-3,5-Me}})(CO)_2$ and $Rh(\kappa^3\text{-}Tp^{3,5\text{-Me}})(CO)_2$ react via a common mechanism.

Calculations. In order to understand the C−H mechanisms further and to try to resolve the apparent discrepancy between the above experimental data and the original mechanism proposed for C-H activation by $Rh(Tp^{3,5\text{-Me}})(CO)_2$, we have performed DFT calculations of the alkane C−H bond activation by $Rh(Tp^{3,5\text{-Me}})(CO)_2$. Larger basis-set calculations on two systems, (i) $Rh(Tp^{3,5\text{-Me}})(CO)(C_2H_6)$, a model for the experimental linear alkane system, and (ii) $Rh(Tp^{3,5\text{-Me}})(CO)(C_6H_{12})$, one of the experimental systems, reveal the detailed reaction mechanism shown in Scheme 3. The relative energies and spectroscopic features are given in Tables 3, 4, and 5, and the structural details are given in Figures 6 and 7. The energies in the text are enthalpies unless otherwise noted. Details of the individual species will be discussed after describing the general features that are common to both systems. Although the new experiments reported here are with the larger $Tp^{4\text{-tBu-3,5-Me}}$ ligand, equally accurate calculations with that ligand were not possible, because the size of the whole system exceeds the computational resources. Furthermore, although important differences are seen with this larger Tp ligand, the overall reaction behavior was similar to that reported previously.

After photodissociation of a CO ligand from $Rh(Tp^{3,5\text{-Me}})$-$(CO)_2$ (**1**), the initially formed unsolvated monocarbonyl species, a κ^3-$Tp^{3,5\text{-Me}}$ molecule with three strong N−Rh bonds (**2** in Scheme 3), can have a triplet (^{3}**2**) or singlet (^{1}**2**) ground state. This monocarbonyl species can then be solvated, forming $Rh(Tp^{3,5\text{-Me}})(CO)(RH)$, where the alkane is weakly bound in an η^1-mode (κ^3-$Tp^{3,5\text{-Me}}/\eta^1$-RH; **3**). Again, there is the possibility of a triplet (^{3}**3**) or a singlet (^{1}**3**) ground state. Species **3** can then rearrange to a species with the alkane strongly bound in an η^2-mode and an elongated "apical" Rh-N bond ($\kappa^{2\,1}/_2$-$Tp^{3,5\text{-Me}}/\eta^2$-RH; **4**). Species **4** has a singlet ground state. The species $\kappa^{2\,1}/_2$-$Tp^{3,5\text{-Me}}/\eta^2$-RH (**4**) can further rearrange to κ^2-$Tp^{3,5\text{-Me}}/\eta^2$-RH (**5**), in which one of the pyrazolyl rings is rotated to eliminate the weak $Rh-N_{apical}$ bond.

Table 2. Activation Parameters and Lifetimes

parent complex Rh(Tp)(CO)$_2$	parameter	*n*-heptane	*n*-decane	cyclohexane
Tp$^{4\text{-tBu-3,5-Me}}$	lifetime of κ^3/κ^2 conversion/ps	236 ± 12	391 ± 15	247 ± 10
	B/**A** ratio at equilibrium	1.4	1.1	2.0
	k_1(**A** → **B**)/10^9 s^{-1}	2.5 ± 0.3	1.3 ± 0.2	2.7 ± 0.5
	k_{-1}(**B** → **A**)/10^9 s^{-1}	1.8 ± 0.2	1.2 ± 0.2	1.3 ± 0.3
	lifetime of C−H activation/ns	28.8 ± 0.5[a]	34.3 ± 0.3[a]	199 ± 12[a]
				954 ± 13[b]
	$\Delta H^{\ddagger}$/kcal mol^{-1}	2.9 ± 0.2	-	4.9 ± 0.2
		n-pentane	*n*-heptane	cyclohexane
Tp$^{3,5\text{-Me}}$	lifetime of C−H activation/ns	6 (±1)[c]	10 (±2)[c]	241 (±1)[b]
	$\Delta H^{\ddagger}$ of C−H activation/kcal mol^{-1}	4.0 (±0.1)	3.2 (±0.1)	5.1 (±0.3)

[a] Saturated under CO at ambient pressure. [b] Saturated under Ar with no added CO. [c] Extrapolated to the temperature of 298 K using the activation parameters.

Scheme 3. Mechanistic Routes from Density Functional Theory Calculations

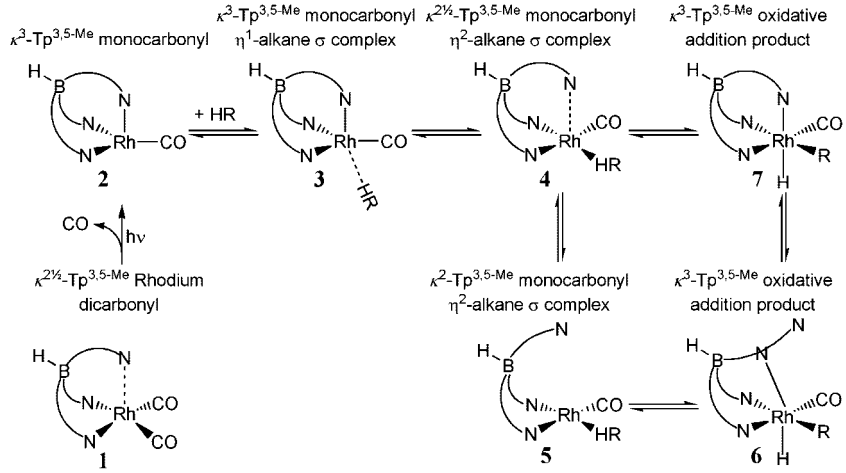

Table 3. Relative Energies (kcal mol^{-1}) and Stretching Frequencies (cm^{-1}) for Rh(Tp$^{3,5\text{-Me}}$)(CO)(C$_2$H$_6$) with B3LYP

Rh(Tp$^{3,5\text{-Me}}$)(CO)(C$_2$H$_6$)	ΔE	ΔE_0	$\Delta H^{o/\ddagger}$	$\Delta G^{o/\ddagger}$	ν_{CO}	ν_{BH}	ν_{RhH}
singlet Rh(κ^3-Tp$^{3,5\text{-Me}}$)(CO); ^{1}**2**	0.0	0.0	0.0	0.0	2044.1	2619.6	
triplet Rh(κ^3-Tp$^{3,5\text{-Me}}$)(CO); ^{3}**2**	−5.99	−6.16	−5.45	−8.43	2045.5	2619.6	
κ^3-Tp$^{3,5\text{-Me}}$/η^1-C$_2$H$_6$; ^{3}**3**	−6.23	−6.06	−4.47	−1.07	2044.0	2624.9	
MECP ^{3}**3**–^{1}**3**	0.54	0.73[a]	3.07[a]	6.47[a]			
κ^3-Tp$^{3,5\text{-Me}}$/η^1-C$_2$H$_6$; ^{1}**3**	−0.97	−0.70	0.66	5.48	2042.5	2618.3	
TS ^{1}**3**–**4**	−0.90	−0.48	0.66	8.34			
$\kappa^{2\,1/2}$-Tp$^{3,5\text{-Me}}$/η^2-C$_2$H$_6$; **4**	−3.88	−2.46	−1.43	6.80	2053.3	2608.0	
TS **4**–**5**	−3.79	−2.43	−1.95	8.48			
κ^2-Tp$^{3,5\text{-Me}}$/η^2-C$_2$H$_6$; **5**	−4.03	−2.50	−1.60	7.65	2060.7	2564.6	
TS **5**–**6**	11.58	10.90	11.40	21.49			
$\kappa^{3'}$-Tp$^{3,5\text{-Me}}$/C$_2$H$_5$/H; **6**	4.15	4.05	4.63	15.19	2096.6	2589.3	2238.9
TS **4**–**7**	7.47	6.95	7.44	17.07			
TS **6**–**7**	6.25	6.26	6.27	18.64			
κ^3-Tp$^{3,5\text{-Me}}$/C$_2$H$_5$/H; **7**	−13.65	−12.48	−12.30	−0.31	2087.6	2630.2	2158.7
TS **4**–**8**	−2.29	−1.02	−0.58	10.14			
κ^2-Tp$^{3,5\text{-Me}}$/η^2-C$_2$H$_6$; **8**	−2.56	−1.32	−0.28	8.10	2068.4	2561.2	

[a] Minimum energy crossing point-relative zero-point energy and thermal corrections calculated from the average of those from singlet and triplet σ-ethane complexes.

Starting from **5** (κ^2-Tp$^{3,5\text{-Me}}$/η^2-RH) one could imagine three routes to the final alkyl hydride product (κ^3-Tp$^{3,5\text{-Me}}$/R/H; **7**). First, the reactions could begin by oxidatively adding the alkane to form κ^3-Tp$^{3,5\text{-Me}}$/R/H, **6** (which has an unusual structure in which the N bound to B is the one bound to the Rh), from which the pyrazolyl ring could rotate back to form the final product **7** in a second step (**5** → **6** → **7**). Second, the reaction could be accomplished in one step by oxidatively adding the alkane with concerted rotation of the pyrazolyl ring (**5** → **7**). Third, the pyrazolyl ring could first rotate to recoordinate the third N, returning the system to species **4**, which could then oxidatively add the alkane as the Rh-N$_{ax}$ bond further strengthens and changes from $\kappa^{2\,1/2}$-Tp$^{3,5\text{-Me}}$ to κ^3-Tp$^{3,5\text{-Me}}$ in the product, **7** (**5** → **4** → **7**).

Ethane. The computational results for the ethane systems, Rh(Tp$^{3,5\text{-Me}}$)(CO)(C$_2$H$_6$), are given in Tables 3 and 4. The optimizations were performed with both B3LYP and BP86 functionals, although not all species were recalculated with the latter functional. The three-dimensional structures of the key species are shown in Figure 6.

Calculations with B3LYP predict the triplet state of the initial unsolvated monocarbonyl species (^{3}**2**) to be lower in energy than the singlet (^{1}**2**) by 5.45 kcal mol^{-1}, while calculations with BP86 predict the triplet to be lower in energy by only 0.57 kcal mol^{-1}. Since it is known that B3LYP overestimates, while BP86 underestimates, the stability of triplet states with respect to the corresponding singlet states,[36] one could estimate that the correct energy difference is between these two values. The calculated

Table 4. Relative Energies (kcal mol^{-1}) and Stretching Frequencies (cm^{-1}) for Rh(Tp$^{3,5\text{-Me}}$)(CO)(C$_2$H$_6$) with BP86

Rh(Tp$^{3,5\text{-Me}}$)(CO)(C$_2$H$_6$)	ΔE	ΔE_0	$\Delta H^{o/\ddagger}$	$\Delta G^{o/\ddagger}$	ν_{CO}	ν_{BH}	ν_{RhH}
singlet Rh(κ^3-Tp$^{3,5\text{-Me}}$)(CO); ^{1}**2**	0.0	0.0	0.0	0.0	1957.6	2553.8	
triplet Rh(κ^3-Tp$^{3,5\text{-Me}}$)(CO); ^{3}**2**	−0.66	−0.59	−0.57	−1.07	1946.3	2550.2	
κ^3-Tp$^{3,5\text{-Me}}$/η^1-C$_2$H$_6$; ^{1}**3**	−0.71	−0.36	−0.31	10.48	1958.5	2548.5	
κ^3-Tp$^{3,5\text{-Me}}$/η^1-C$_2$H$_6$; ^{3}**3**	−0.67	−0.39	0.64	5.38	1945.5	2555.9	
TS ^{1}**3**–**4**	−0.32	0.04	0.45	10.61			
$\kappa^{2\,1}/_2$-Tp$^{3,5\text{-Me}}$/η^2-C$_2$H$_6$; **4**	−3.21	−1.96	−1.54	8.60	1968.1	2380.1	
κ^2-Tp$^{3,5\text{-Me}}$/η^2-C$_2$H$_6$; **5**	−2.95	−1.74	−1.37	9.02	1975.5	2407.8	
$\kappa^{3'}$-Tp$^{3,5\text{-Me}}$/C$_2$H$_5$/H; **6**	−0.59	−0.83	−0.69	10.85	2003.9	2527.3	2183.1
TS **4**–**7**	2.09	1.61	1.52	13.44			
κ^3-Tp$^{3,5\text{-Me}}$/C$_2$H$_5$/H; **7**	−18.9	−17.75	−18.09	−4.63	1998.5	2558.1	2109.0

Table 5. Relative Energies (kcal mol^{-1}) and Stretching Frequencies (cm^{-1}) for Rh(Tp$^{3,5\text{-Me}}$)(CO)(C$_6$H$_{12}$) with B3LYP

Rh(Tp$^{3,5\text{-Me}}$)(CO)(C$_6$H$_{12}$)	ΔE	ΔE_0	$\Delta H^{o/\ddagger}$	$\Delta G^{o/\ddagger}$	ν_{CO}	ν_{BH}	ν_{RhH}
singlet Rh(κ^3-Tp$^{3,5\text{-Me}}$)(CO); ^{1}**2**	0.0	0.0	0.0	0.0	2052.5	2617.4	
triplet Rh(κ^3-Tp$^{3,5\text{Me}}$)(CO); ^{3}**2**	−6.00	−6.00	−6.00	−6.00	2055.2	2618.5	
κ^3-Tp$^{3,5\text{-Me}}$/η^1-C$_6$H$_{12}$; ^{1}**3**	0.24	0.66	1.96	10.55	2046.5	2618.6	
κ^3-Tp$^{3,5\text{-Me}}$/η^1-C$_6$H$_{12}$; ^{3}**3**	−5.02	−4.70	−3.13	3.00	2052.4	2622.4	
$\kappa^{2\,1}/_2$-Tp$^{3,5\text{-Me}}$/η^2-C$_6$H$_{12}$; **4**	−2.31	−1.03	−0.26	11.41	2055.4	2550.1	
TS **4**–**5**	−2.26	−1.14	−0.98	13.27			
κ^2-Tp$^{3,5\text{-Me}}$/η^2-C$_6$H$_{12}$; **5**	−2.62	−1.28	−0.67	12.23	2064.4	2503.9	
TS **4**–**7**	11.20	10.33	10.67	24.64			
TS **5**–**6**	13.75	13.05	13.24	27.93			
$\kappa^{3'}$-Tp$^{3,5\text{-Me}}$/C$_6$H$_{11}$/H; **6**	13.23	12.92	13.24	28.18	2096.9	2587.0	2232.3
κ^3-Tp$^{3,5\text{-Me}}$/C$_6$H$_{11}$/H; **7**	−9.22	−8.51	−8.41	7.09	2091.7	2626.9	2175.6

ν_{CO} frequencies of triplet and singlet with B3LYP differ by only 1 cm^{-1}, while with BP86 the difference is 10 cm^{-1}. For the weakly solvated species (**3**) with B3LYP the triplet state is lower in energy than the singlet (^{1}**3**) by 5.13 kcal mol^{-1}, while with BP86 the singlet is the ground state with the triplet 0.95 kcal mol^{-1} higher in energy. The pattern of ν_{CO} changes is similar to that calculated for **2**.

The solvated monocarbonyl, **3**, rearranges to species **4** ($\kappa^{2\,1}/_2$-Tp$^{3,5\text{-Me}}$/η^2-C$_2$H$_6$). Species **4** has a singlet ground state, and it is 3.04 kcal mol^{-1} higher in energy than ^{3}**3** in the B3LYP calculations, but 1.23 kcal mol^{-1} lower in energy than ^{1}**3** in BP86 calculations. If **3** has a triplet ground state, then the formation of **4** would involve a triplet−singlet potential energy surface crossing. Using the method of Harvey,[30] we determined that the minimum energy crossing point (MECP) is 7.47 kcal mol^{-1} above ^{3}**3** for the Rh(Tp$^{3,5\text{-Me}}$)(CO)(C$_2$H$_6$) model system. However, if **3** has a singlet ground state, as predicted by BP86, then the formation of **4** would occur on the singlet surface and the singlet-surface barrier is predicted to be less than 1 kcal mol^{-1} by both B3LYP and BP86.

The $\kappa^{2\,1}/_2$-Tp$^{3,5\text{-Me}}$/η^2-C$_2$H$_6$ (**4**) species is connected by a very small barrier to a related κ^2-Tp$^{3,5\text{-Me}}$/η^2-C$_2$H$_6$ (**5**) species. Species **5** is slightly lower in energy than **4** with B3LYP and slightly higher in energy than **4** with BP86. Species **8** (a conformer of **5**, not shown in the Figure) has the pyrazolyl ring rotated in the opposite direction and is slightly more than 1 kcal mol^{-1} higher in energy. The barrier between **4** and **8** (**TS 4**-**8**) is 1.44 kcal mol^{-1}. For both B3LYP and BP86, the difference in the calculated ν_{CO} between the κ^3-Tp$^{3,5\text{-Me}}$/η^1-C$_2$H$_6$ (**3**) and the κ^2-Tp$^{3,5\text{-Me}}$/η^2-C$_2$H$_6$ (**5**) is ∼17 cm^{-1}, in agreement with the difference experimentally observed between species **A** and **B**, 18 cm^{-1}.[6,8] The calculated ν_{CO} band of the species $\kappa^{2\,1}/_2$-Tp$^{3,5\text{-Me}}$/η^2-C$_2$H$_6$ (**4**) is at nearly the same position as the calculated strong band of the starting dicarbonyl (**1**). Thus, the overlap of these ν_{CO} bands would prevent the observation of **4**.

The next steps of the reaction involve breaking of the C−H bond by oxidative addition to Rh and shortening of the third Rh−N bond to give the final alkyl hydride product, κ^3-Tp$^{3,5\text{-Me}}$/C$_2$H$_5$/H (**7**). The C−H bond-breaking step can occur from the species κ^2-Tp$^{3,5\text{-Me}}$/η^2-C$_2$H$_6$ (**5**) by oxidatively adding the C−H bond without reforming the Rh−N$_{apical}$ bond. In spite of a starting geometry with a κ^2-Tp$^{3,5\text{-Me}}$ ligand, the final geometry of the Tp$^{3,5\text{-Me}}$ ligand for **6** optimized to an unexpected structure, in which the nitrogen atom bound to boron appears to be π bonded to the Rh (Figure 6). The calculated energy of the transition state (TS) between the κ^2-Tp$^{3,5\text{-Me}}$/η^2-C$_2$H$_6$ (**5**) and **6** shows a moderately high activation barrier of 13.0 kcal mol^{-1}. If this alkyl hydride species (**6**) formed first, it could give the final alkyl hydride product κ^3-Tp$^{3,5\text{-Me}}$/C$_2$H$_5$/H (**7**) by rotating the pyrazolyl ring of the Tp$^{3,5\text{-Me}}$. The barrier for this latter process is low, 1.64 kcal mol^{-1}.

The calculations on the simpler model RhTp(CO)(CH$_4$) show that there is no direct TS between κ^2-Tp/η^2-CH$_4$ (**5**) and the final product (**7**); a second-order saddle point was the only critical point found on the potential energy surface on the direct route between **5** and **7**. However, a lower energy path was found that involves κ^2-Tp$^{3,5\text{-Me}}$/η^2-C$_2$H$_6$ (**5**) first returning to the $\kappa^{2\,1}/_2$-Tp$^{3,5\text{-Me}}$/η^2-C$_2$H$_6$ (**4**) structure. From **4** the barrier to the final product (**7**) is only 8.87 kcal mol^{-1}, which is lower than the barrier calculated for the **5** → **6** → **7** pathway. Therefore, **5** → **4** → **7** is the lowest energy pathway for the reaction.

The product species (**7**) has the lowest energy of all the species for this system; the overall exothermicity with respect to separated reactants is 12.30 kcal mol^{-1} for the singlet state and 6.85 kcal mol^{-1} for the triplet state of the reactants with B3LYP, whereas BP86 afforded 18.09 kcal mol^{-1} for the singlet and 17.52 kcal mol^{-1} for the triplet. As expected the triplet state of the product is very high in energy. There is also another conformer (**7′**) of the product, where the ethyl group has a different orientation; **7′** is higher in energy by 1.03 kcal mol^{-1}.

(36) (a) Fan, Y.; Hall, M. B. *Chem.-Eur. J.* **2004**, *10*, 1805–1814. (b) Cavallo, L.; Jacobsen, H. *Eur. J. Inorg. Chem.* **2003**, *892*, 902. (c) de Visser, S. P.; Ogliaro, F.; Sharma, P. K.; Shaik, S. *J. Am. Chem. Soc.* **2002**, *124*, 11809–11826. (d) de Visser, S. P.; Ogliaro, F.; Harris, N.; Shaik, S. *J. Am. Chem. Soc.* **2001**, *123*, 3037–3047. (e) Harris, N.; Cohen, S.; Filatov, M.; Ogliaro, F.; Shaik, S. *Angew. Chem., Int. Ed.* **2000**, *39*, 2003–2007. (f) Schroder, D.; Shaik, S.; Schwarz, H. *Acc. Chem. Res.* **2000**, *33*, 139–145. (g) Harvey, J. N. *Struct. Bonding (Berlin)* **2004**, *112*, 151–183. (h) Salomon, O.; Reiher, M.; Hess, B. A. *J. Chem. Phys.* **2002**, *117*, 4729–4737.

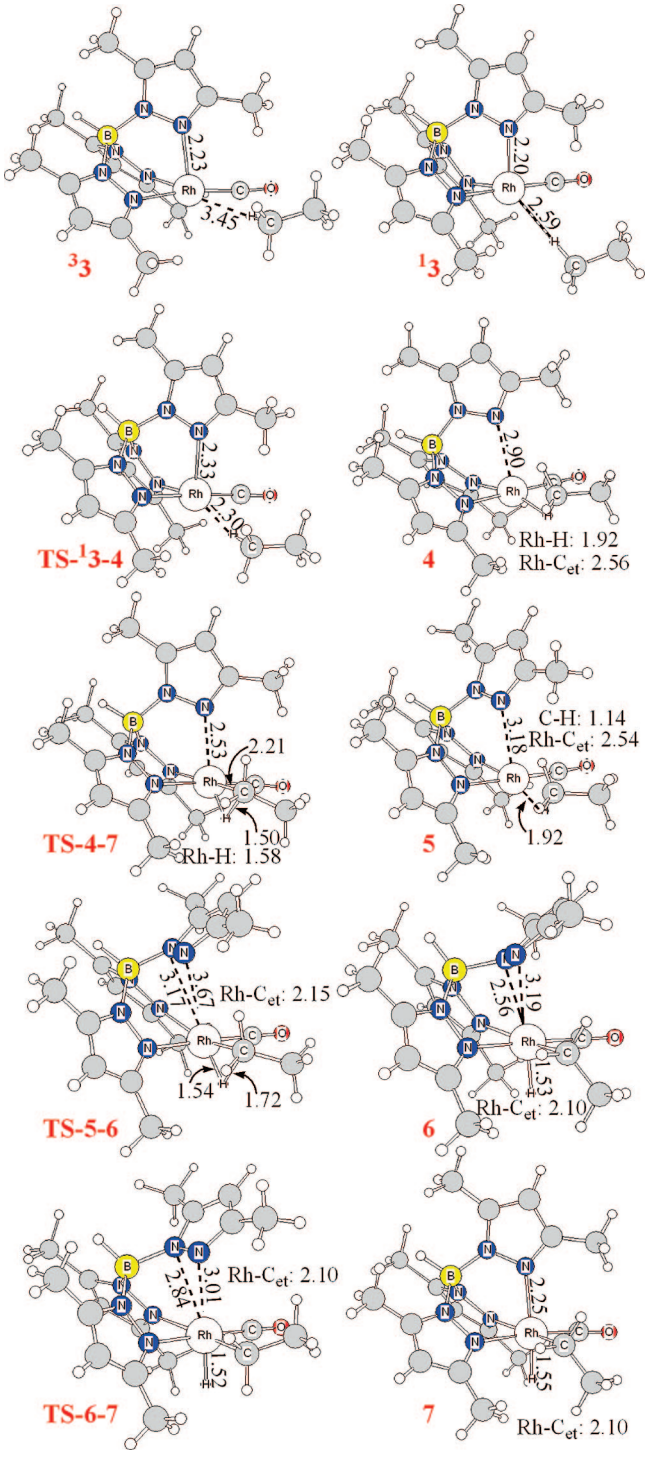

Figure 6. B3LYP-optimized three-dimensional structures for species in the Rh(Tp$^{3,5\text{-Me}}$)(CO)(C$_2$H$_6$) reaction.

Cyclohexane. We also calculated the most important species in the reaction pathway for the experimental systems, Rh(Tp$^{3,5\text{-Me}}$)(CO)(C$_6$H$_{12}$), with B3LYP (Table 5, Figure 7). The unsolvated monocarbonyl species are the same as those for ethane; the small difference in calculated values is a consequence of a slightly different basis set. In this case ^{3}**2** is again lower in energy than ^{1}**2** (6.00 kcal mol^{-1}) and the calculated ν_{CO} frequencies differ by only 2.7 cm^{-1}. For the alkane-solvated monocarbonyl species (**3**) the triplet ground state (^{3}**3**) is also lower in energy than the singlet (^{1}**3**) by 5.09 kcal mol^{-1}. The ν_{CO} frequencies of the triplet and singlet differ by about 5.9 cm^{-1}, which is a slightly larger difference than that calculated for ethane with B3LYP.

The $\kappa^{2\,1/2}$-Tp$^{3,5\text{-Me}}$/η^2-C$_6$H$_{12}$ species (**4**) with cyclohexane strongly bound in η^2-mode and an elongated "apical" Rh−N bond has a singlet ground state and is 2.87 kcal mol^{-1} higher in energy than ^{3}**3**, which is similar to findings in B3LYP calculations with ethane. As in the case of ethane the calculated ν_{CO} band of species **4** is at nearly the same position as the calculated strong band of starting dicarbonyl **1**, and their overlap would prevent the observation of **4**.

Because of the very large size of this system, it was prohibitively expensive to calculate the triplet-singlet crossing barrier between triplet κ^3-Tp$^{3,5\text{-Me}}$/η^2-C$_6$H$_{12}$ (^{3}**3**) and singlet $\kappa^{2\,1/2}$-Tp$^{3,5\text{-Me}}$/η^2-C$_6$H$_{12}$ (**4**). However, the similarity of other barriers in this region of the reaction paths suggests that it would not be too different from those calculated above for the Tp$^{3,5\text{-Me}}$/C$_2$H$_6$ system.

The κ^2-Tp$^{3,5\text{-Me}}$/η^2-C$_6$H$_{12}$ (**5**) species is slightly lower in energy than **4**, 0.41 kcal mol^{-1}. The difference in calculated ν_{CO} between **3** and **5** (12 cm^{-1}) is in reasonable agreement with the difference experimentally observed between the species **A** and **B** (18 cm^{-1}).[6]

In the model system with ethane, the lowest energy pathway for the formation of the final alkyl hydride product, κ^3-Tp$^{3,5\text{-Me}}$/η^2-C$_6$H$_{11}$/H (**7**), involves **5** returning to **4** and **4** going to the final product (**7**) in a single step. The TS for this step (**TS 4-7**) with cyclohexane has a barrier of 10.93 kcal mol^{-1}. This higher barrier, in comparison to that calculated for ethane, is in agreement with experimental data (Table 2), which show cycloalkanes (secondary C−H bonds) having slower reaction rates and higher barriers than linear alkanes, where oxidative addition occurs at the primary C−H bonds.

In the alternative higher energy pathway, starting from **5**, the consecutive breaking of the C−H bond and the reforming of the Rh−N bond to give the final product (**7**), species **6** is found with a structure like that for the reaction involving ethane. However, **6** is higher in energy than **5** by 13.91 kcal mol^{-1}, and thus, this intermediate (**6**) is even higher in energy than the TS on the most favorable path, **TS 4-7**.

As it was calculated for the ethane system, the product in this reaction is the lowest energy species and the overall exothermicity is 8.41 kcal mol^{-1} with respect to separated Rh(Tp$^{3,5\text{-Me}}$)(CO) and cyclohexane in the singlet state. The exothermicity reduces to 2.41 kcal mol^{-1} with respect to the triplet.

Discussion

Reaction of Linear Alkanes vs Cyclohexane. The TRIR measurements for both Rh(κ^3-Tp$^{4\text{-tBu-3,5-Me}}$)(CO)$_2$ and Rh(κ^3-Tp$^{3,5\text{-Me}}$)(CO)$_2$ show that the rate of C−H activation in cyclohexane is much slower than in the *n*-alkanes heptane and decane; the former has activation enthalpies ∼2 kcal mol^{-1} higher than the latter (Table 2). Although, the majority of the computational results were obtained by the B3LYP method, which predicts barriers that are somewhat too high (Tables 3 and 4), the relative enthalpies of activation between primary and secondary C−H bond activation are predicted quite well at ∼3 kcal mol^{-1} (see Tables 3 and 5). The difference in rates can be interpreted in terms of the presence of primary C−H bonds in the systems with the linear alkanes. However, other factors also influence this reaction. These include the strength of metal−alkane interaction, which may affect the concentration of species undergoing the oxidative-addition reaction. The difference in the lifetime of C−H activation between linear and

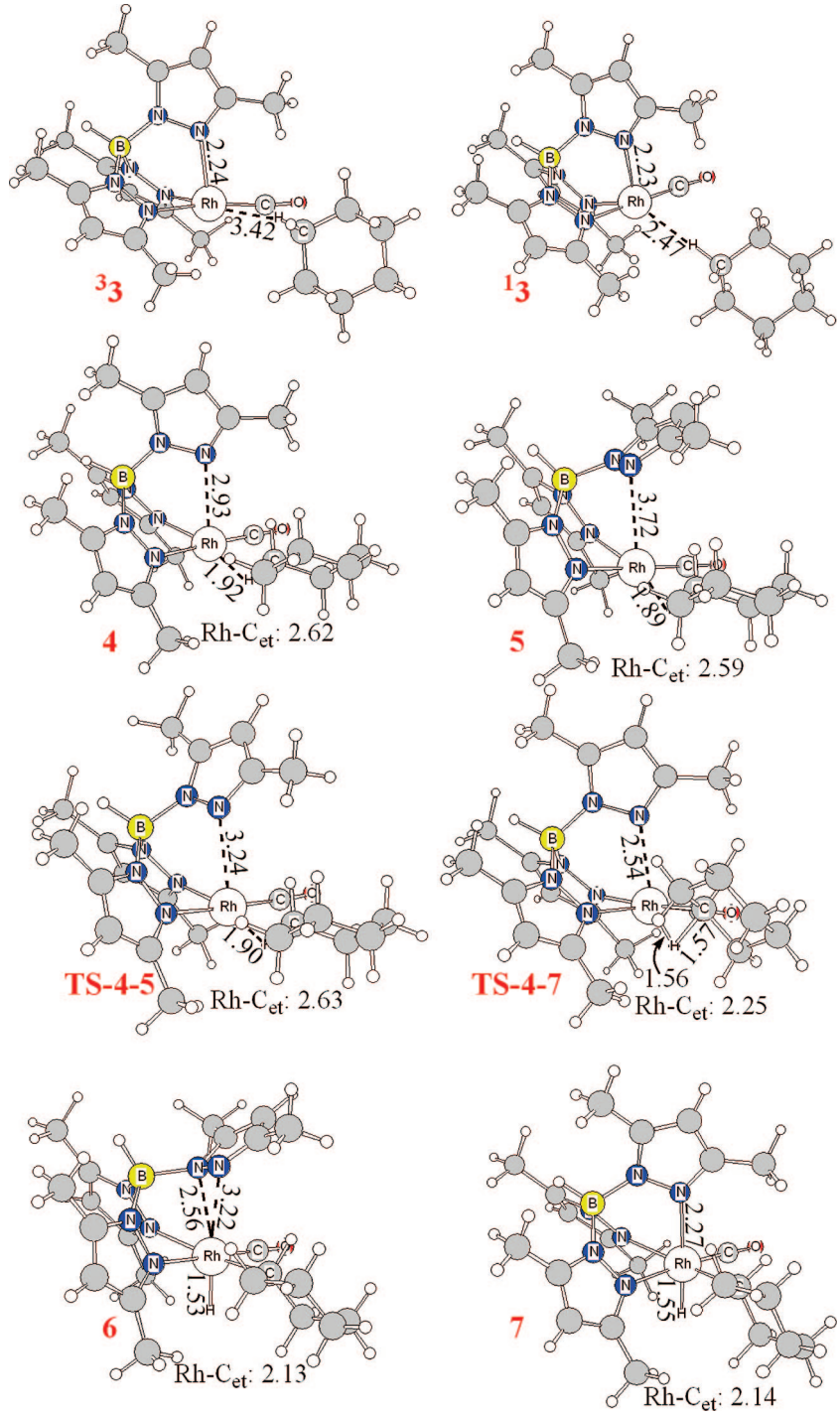

Figure 7. B3LYP-optimized three-dimensional structures for species in the Rh(Tp$^{3,5\text{-Me}}$)(CO)(C$_6$H$_{12}$) reaction.

branched alkanes (e.g., $k_{cyclohexane}/k_{heptane}$ ca. 30–40) as reported in this study is similar to those predicted from competition experiments on Rh(Tp$^{3,5\text{-Me}}$)(CN-neopentyl)$_2$, where C−H activation of secondary alkanes was estimated to be ca. 10 times slower than a primary C−H bond.[8]

Reaction Mechanism. The TRIR measurement on Rh(κ^3-Tp$^{4\text{-tBu-3,5-Me}}$)(CO)$_2$ and Rh(κ^3-Tp$^{3,5\text{-Me}}$)(CO)$_2$ and the larger basis set calculations on the model system Rh(Tp$^{3,5\text{-Me}}$)(CO)(C$_2$H$_6$) and on one of the experimental systems, Rh(Tp$^{3,5\text{-Me}}$)(CO)(C$_6$H$_{12}$), revealed the detailed reaction mechanism shown in Scheme 3 and Figure 8. Here, we will integrate the experimental and theoretical results and discuss them from the perspective of those species involved in the reaction.

Species A. After photodissociation the initially unsolvated monocarbonyl species (**2**) (Figures 6 and 7) is rapidly solvated by alkane-forming species **A** (Figures 2, 3, and 4). By comparison of experimental and computational results, **A** can be assigned to Rh(κ^3-Tp$^{3,5\text{-Me}}$)(CO)(η^1-RH), **3**. Although the alkane is only weakly bound to the Rh, we assume that in liquid alkane the majority species is the solvated form, not the unsolvated monocarbonyl, but **A** could be an equilibrium mixture of these two species, which are predicted to have essentially the same stretching frequencies (Tables 3, 4, and 5). However, it is unclear at this point whether **A** has a singlet or triplet ground state. B3LYP, which is known to favor triplet states, predicts that the triplet is lower in energy than the singlet

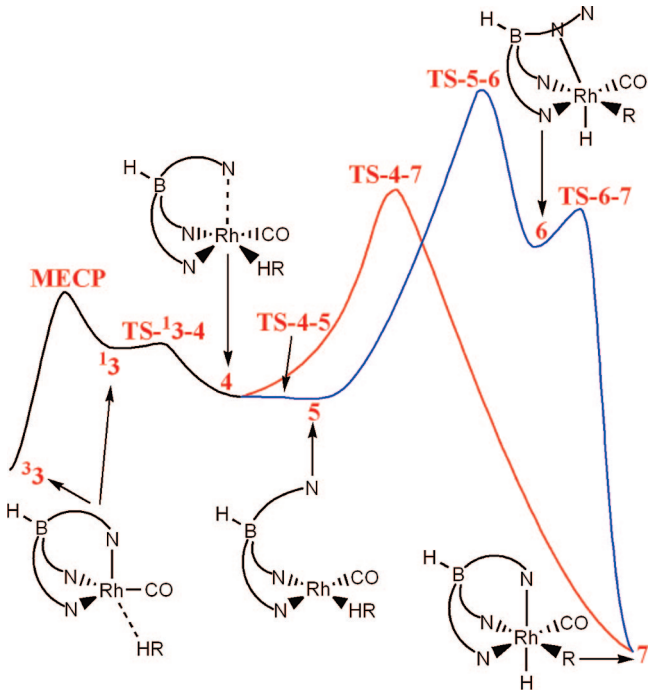

Figure 8. Energy diagram summarizing the mechanistic route for C−H bond activation from the density functional calculations. The results from this work lead to the conclusino that ^{3}**3** is species A, **5** is species B, **4** is species C, and **7** is species D.

by 5–6 kcal mol^{-1}. In contrast, BP86, which is known to overstabilize singlet states, predicts that the two states are of nearly equal energy. Thus, we are presented with a dilemma. From theoretical considerations alone we would estimate that the ground-state is a triplet with its stability somewhere between those calculated from B3LYP and BP86 functionals.

In a previous publication the free-energy barrier for the reaction of **A** was estimated to be ∼4.3 kcal mol^{-1} by using the experimental lifetime and applying simple transition-state theory. Here, similar lifetimes were determined experimentally for the Rh/Tp$^{4\text{-tBu-3,5-Me}}$ system, but **A** was determined to decay to an equilibrium mixture of **A** and **B**. Further support for the conclusion that **A** is a triplet is provided by these experimental barriers in the following way. Both functionals (B3LYP and BP86) predict that this barrier would be less than 1 kcal mol^{-1} if **A** was a singlet. However, if **A** is a triplet, then the calculations predict a significant barrier for **A** → **B**. Thus, the only way to account for the evidence of a barrier between **A** and **B** is to assume that **A** is a triplet (^{3}**3**). By using the experimental barrier, it can be estimated that B3LYP is overestimating the stability of the triplet by ∼3.2 kcal mol^{-1}, as this is the value needed to bring the calculated barrier of ∼7.5 kcal mol^{-1} from the B3LYP triplet-singlet crossing point into coincidence with the experimental ones.

Species B. The solvated monocarbonyl **A** then rearranges to species **B**, which is more stable in the Tp$^{3,5\text{-Me}}$ system and of similar stability in the Tp$^{4\text{-tBu-3,5-Me}}$ system. The calculations predict two species with a strongly bound η^2-alkane: one with an elongated "apical" Rh-N bond ($\kappa^{2\,1}/_{2}$-Tp/η^2-RH; **4**) and another with a rotated (twisted) pyrazolyl ring (κ^2-Tp/η^2-RH; **5**). Species **4** and **5** have singlet ground states within ∼1 kcal mol^{-1} of each other and are separated by a very small barrier. The ν_{CO} band positions provide good clues to decide on the nature of **B** being either **4** or **5**. The calculated ν_{CO} for **4** is strikingly similar to a calculated strong ν_{CO} band of the starting material (**1**). Thus, **4** would be difficult to observe. Furthermore, the calculated difference in the ν_{CO} between the κ^3-Tp/η^1-RH (**3**) and the κ^2-Tp/η^2-RH (**5**) is 12–18 cm^{-1}, in reasonable agreement with the difference experimentally observed between the species **A** and **B** in previous experimental results (18 cm^{-1})[6] and with the data in this paper (20–22 cm^{-1}). It is also in agreement with our previous prediction[7] and with experimental data on Rh(Bp$^{3,5\text{-Me}}$)(CO),[6b] which under similar conditions show only intermediate **B**, a result interpreted as proving that **A** has a κ^3-Tp, while **B** has a κ^2-Tp. The difference in observed equilibria between the Tp$^{3,5\text{-Me}}$ and the Tp$^{4\text{-tBu-3,5-Me}}$ systems results from the steric bulk of the ^{t}Bu group, which makes the species with the rotated pyrazol ring (**5**) less stable for Tp$^{4\text{-tBu-3,5-Me}}$.

Species C. In the previously proposed mechanism,[6] the C−H bond-breaking step occurs from intermediate **B**, the κ^2-Tp/η^2-RH species **5**, with a barrier of ∼8.3 kcal mol^{-1}. These authors proposed that C−H bond breaking occurs, first forming an "activated complex", a κ^2-Tp/R/H species named **C**, which then reforms the Rh−N$_{apical}$ bond to stabilize the final product, **D**. As in the previous experiments[6b] we have not been able to observe intermediate **C**. Our results, however, have demonstrated that an equilibrium mixture of **A**[Rh(κ^3-Tp$^{4\text{-tBu-3,5-Me}}$)(CO)(RH)] and **B**[Rh(κ^2-Tp$^{4\text{-tBu-3,5-Me}}$)(CO)(RH)] exists in solution. However, which species, **A** or **B**, is the intermediate that leads to C−H activation cannot be determined from our experiments. Since in the previously proposed mechanism[6b] **B** is the intermediate that leads to C−H activation, we computationally probed the pathway for that process.

A concerted mechanism can be considered, in which the C−H oxidative addition and the reformation of the third Rh−N bond happened simultaneously from κ^2-Tp/η^2-RH (**5**) through a single TS. This mechanism is consistent with the experimental results, as the proposed species **C** has not been observed. In spite of numerous searches for a single TS in several basis sets, functionals, and models, we were only able to identify a second-order saddle point (a local maximum) connecting **B**, κ^2-Tp/η^2-RH (**5**), and the product **D**, κ^3-Tp/R/H (**7**). Thus, we exclude this concerted mechanism from further consideration.

The oxidative addition of the C−H bond without the reformation of the Rh−N$_{apical}$ bond produces an alkyl hydride like the previously postulated[6b] species **C**. In spite of a starting geometry with the κ^2-mode for the Tp ligand, the final geometry of this alkyl hydride species, **6**, optimized to an unexpected structure, in which the nitrogen atom bound to the boron is π bonded to the Rh (Figures 6 and 7). Hence, oxidative addition does not occur in the complex with the Tp ligand in κ^2-mode as the additional donor strength of a third N donor is required for the reaction to proceed. Furthermore, in spite of finding a species **6**, which appears to be similar to the proposed species **C**, a barrier of 13.0 kcal mol^{-1} along this route appears too high by ∼4 kcal mol^{-1} when compared to the alternate route from species **4**.

Alternatively, the Rh−N$_{apical}$ bond could reform first, and then C−H activation could occur to reach the final product. In this route species **B** [κ^2-Tp/η^2-RH (**5**)] first returns to the unobserved $\kappa^{2\,1}/_{2}$-Tp/η^2-RH (**4**) species, which then oxidatively adds the C−H bond while strengthening the partially reformed Rh−N$_{apical}$ bond to reach the final product **D**, κ^3-Tp/R/H (**7**). This route is in agreement with our experimental data, as it easily explains how both **A** and **B**, which are in equilibrium, form the product (**D**) at the same rate. The predicted third, yet unobserved intermediate $\kappa^{2\,1}/_{2}$-Tp/η^2-RH (**C**), which is in equilibrium with both **A** and **B**, provides the single path over the rate-determining barrier,

allowing **A** and **B** to decay simultaneously. This last route has the lowest lying TS of any route to the final product **D** (**7**). The B3LYP calculations overestimate this barrier, but as expected from other work on C−H bond activation[37] the BP86 value may be closer to those found experimentally. The calculated enthalpic barrier for **TS 4–7** provided by BP86 is 2.9 kcal mol^{-1}, which is very close to the measured values of 2.9, 3.2, and 4.0 kcal mol^{-1} for the linear alkane systems reported in this work (Table 2). Since this TS (**TS 4–7**) has a calculated barrier much lower than that for the **TS 5–6**, between **B**, κ^2-Tp/η^2-RH (**5**), and the alkyl hydride species with a rotated pyrazolyl ring (**6**), the former pathway is concluded to be the mechanism for this reaction. Furthermore, for cyclohexane as substrate the *intermediate* formed when oxidative addition occurs first (**6**) is actually higher in energy than the TS for the conversion of **4** to the product. Thus, species **C**, previously postulated[6b] as a complex in which the C−H bond breaking had already occurred, is actually the unobserved $\kappa^{2\,1/2}$-Tp/η^2-RH (**4**) species, which has the third N partially recoordinated but the C−H bond still intact. This situation is reminiscent of other reactions[38] where the product is formed from an unobserved less stable intermediate (**4**) rather than from the observed more stable ones (**3** and **5**). Based on our calculated energies, species **C** might best be viewed as a metastable intermediate that connects the pyrazolyl ring rotation to the TS for C−H bond activation.

Conclusions

On the basis of TRIR experiment and DFT calculations the detailed reaction mechanism of alkane C−H activation by tris(pyrazolyl)borato carbonyl rhodium has been elucidated fully. The mechanism of this archetypical C−H activation reaction is summarized in Scheme 3 and Figure 8. Photolysis of Rh($\kappa^{2\,1/2}$-Tp)(CO)$_2$ in alkane solution promptly produces an intermediate (**A**) with weakly coordinated alkane, Rh(κ^3-Tp)(CO)−(RH), which is predicted to be in the triplet state from DFT calculations. The calculations further predict that the first barrier arises from the triplet-singlet surface crossing. The first intermediate on the singlet surface is Rh($\kappa^{2\,1/2}$-Tp)(CO)(RH), which has one of the Tp arms partially detached, one weak Rh−N bond, and a strongly bound alkane. This intermediate was not observed in TRIR experiments, as it has a ν_{CO} equal to that of the parent dicarbonyl. Further rotation of the Tp arm and complete breaking of the Rh−N bond give the second observed intermediate (**B**), Rh(κ^2-Tp)(CO)(RH). Depending on the nature of the Tp ligand, these two observed species are in rapid equilibrium with each other and on the basis of the DFT results also with the unobserved Rh($\kappa^{2\,1/2}$-Tp)(CO)(RH). The DFT calculations predict that this unobserved complex, Rh($\kappa^{2\,1/2}$-Tp)CO(RH), is the C−H activating species, producing final alkyl hydride product Rh(κ^3-Tp)(CO)(R)H. This prediction provides a clear reason for the observation that in the case of Tp$^{4\text{-tBu-}3,5\text{-Me}}$ **A** and **B** produce product at the same rate.

This mechanism is also supported by qualitative chemical-bonding considerations for transition metal complexes. After photolysis of starting Rh($\kappa^{2\,1/2}$-Tp)(CO)$_2$ in alkane solution, Rh(κ^3-Tp)(CO)−(RH) is formed, the observed **A**. This species is stable on the triplet surface because it has one electron at the vacant site and one electron in a Rh−N antibonding orbital. The tendency to weaken the coordination of one pyrazolyl ring increases in the singlet state because both electrons are in the Rh−N antibonding orbital. In other words, this singlet d^8 complex is too electron rich since the electron density on Rh increases after losing a CO ligand, a strong π-acceptor, and so to reduce the electron density on the metal, one of the chelating arms of Tp decoordinates. This decoordination and reduction in electron density on Rh promotes a stronger binding of the alkane. The degree of decoordination can be partial, producing Rh($\kappa^{2\,1/2}$-Tp)(CO)(RH), or complete, producing Rh(κ^2-Tp)(CO)(RH), which is the observed **B**. One can expect that Rh($\kappa^{2\,1/2}$-Tp)(CO)(RH) will be unobservable. In TRIR spectra, the bands due to intermediates Rh(κ^3-Tp)(CO)(RH) (**A**) and Rh(κ^2-Tp)(CO)(RH) (**B**) are on either side of one band of the parent dicarbonyl, Rh($\kappa^{2\,1/2}$-Tp)(CO)$_2$. The band of Rh(κ^3-Tp)(CO)(RH) (**A**) has a lower frequency since κ^3-Tp is stronger donor, while Rh(κ^2-Tp)(CO)(RH) (**B**), with the weaker κ^2-Tp donor, has a higher frequency. The Rh($\kappa^{2\,1/2}$-Tp)(CO)(RH), with intermediate donor, $\kappa^{2\,1/2}$-Tp, must therefore have an intermediate frequency, which consequently has a frequency very near that of the parent band.

Among the three alkane intermediates, one with κ^3-Tp, one with $\kappa^{2\,1/2}$-Tp, and the third with κ^2-Tp, the complex with $\kappa^{2\,1/2}$-Tp is activating the C−H bond. It is poised to produce the product, as it has an intermediate electron density on Rh, enabling the coordination center to bind an alkane strongly, and to increase the electron density as needed for the C−H bond activation. It has less electron density on Rh than the κ^3-Tp complex, which only weakly binds alkane. Although the complex with κ^2-Tp can strongly bind alkane, it cannot cleave the C−H bond, as there is not enough electron density on Rh. It is this lack of electron density on Rh that prevents Rh(κ^2-Bp$^{3,5\text{-Me}}$)(CO)(alkane) (Bp = hydrobis(pyrazol-1-yl)borate) species from activating the C−H bond. In previous experiments C−H activation was not observed with the Bp ligand, as coordination of the third arm of the Tp ligand is necessary for C−H bond activation. The intermediate with $\kappa^{2\,1/2}$-Tp coordination has sufficient electron density to start the cleavage of the C−H bond and can easily get more electron density by making the third Rh−N bond shorter. Even in the case of the higher energy pathway, where an alkyl hydride product is obtained from Rh(κ^2-Tp)(CO)(RH), there is the intermediate with a broken C−H bond and unexpected geometry in which the nitrogen atom bound to boron appears to be π-bonded to the Rh, giving additional electron density to Rh.

Acknowledgment. We are especially grateful to Professor W. D. Jones for helpful discussions. We thank Professor A. W. Parker, Dr. P. Matousek, and Mr. A. J. Cowan for advice or assistance in the TRIR experiments. We acknowledge support from the EU (MEIF-CT-2003-502440), EPSRC (GR/R02863), National Science Foundation (CHE-0501874 and DMS-0216275), The Welch Foundation (A-0648), and the Foundation of the Serbian Ministry of Science (142037).

Supporting Information Available: The crystallographic CIF file of Rh(Tp$^{4\text{-tBu-}3,5\text{-Me}}$)(CO)$_2$ and the complete references for Gaussian 03 and Gaussian 98 are available free of charge via the Internet at http://pubs.acs.org.

OM7008217

(37) Hall, M. B.; Fan, H.-J. *Adv. Inorg. Chem.* **2003**, *54*, 321–349.
(38) (a) Chan, A. S. C.; Pluth, J. J.; Halpern, J. *J. Am. Chem. Soc.* **1980**, *102*, 5952–5954. (b) Halpern, J. *Science* **1982**, *217*, 401–407. (c) Landis, C. R.; Halpern, J. *J. Am. Chem. Soc.* **1987**, *109*, 1746–1754.